

CLuP practically achieves ~ 1.77 positive and ~ 0.33 negative Hopfield model ground state free energy

MIHAILO STOJNIC *

Abstract

We study algorithmic aspects of finding n -dimensional *positive* and *negative* Hopfield (\pm Hop) model ground state free energies. This corresponds to classical maximization of random positive/negative semi-definite quadratic forms over binary $\left\{\pm\frac{1}{\sqrt{n}}\right\}^n$ vectors. The key algorithmic question is whether these problems can be computationally efficiently approximated within a factor ≈ 1 . Following the introduction and success of *Controlled Loosening-up* (CLuP-SK) algorithms in finding near ground state energies of closely related Sherrington-Kirkpatrick (SK) models [82], we here propose a CLuP \pm Hop counterparts for \pm Hop models. Fully lifted random duality theory (fl RDT) [78] is utilized to characterize CLuP \pm Hop *typical* dynamics. An excellent agreement between practical performance and theoretical predictions is observed. In particular, for n as small as few thousands CLuP \pm Hop achieve ~ 1.77 and ~ 0.33 as the ground state free energies of the positive and negative Hopfield models. At the same time we obtain on the 6th level of lifting (6-spl RDT) corresponding theoretical thermodynamic ($n \rightarrow \infty$) limits ≈ 1.7784 and ≈ 0.3281 . This positions determining Hopfield models near ground state energies as *typically* easy problems. Moreover, the very same 6th lifting level evaluations allow to uncover a fundamental intrinsic difference between two models: +Hop's near optimal configurations are *typically close* to each other whereas the $-$ Hop's are *typically far away*.

Index Terms: Hopfield models; CLuP algorithm; Fully lifted random duality theory.

1 Introduction

Taking an integer $n \in \mathbb{N}$ and matrix $A \in \mathbb{R}^{n \times n}$ we are interested in the following quadratic form optimization

$$\max_{\mathbf{x} \in \mathbb{B}^n} \mathbf{x}^T A \mathbf{x}, \quad (1)$$

where \mathbb{B}^n are the vertices of the following n -dimensional “binary” cube

$$\mathbb{B}^n \triangleq \left\{ \mathbf{x} \mid \mathbf{x} \in \mathbb{R}^n, \mathbf{x}_i^2 = \frac{1}{n} \right\}. \quad (2)$$

Being one of the foundational problems of the classical NP complexity theory, (1) is hard to approximate within a $\log(n)^{\text{const.}}$ factor [7] (for further considerations including relaxations of integer constraints, see, e.g., [19, 44]). While NP concepts are a useful generic computational complexity guideline, their *worst case* nature might leave them somewhat inconvenient when it comes to proper addressing of *typical* solvability. There indeed may be few bad instances of (1) that are unsolvable in polynomial time, but there is no guarantee that the same scenario repeats itself for a sizeable portion (or even less so for a majority) of all instances. In other words, hardness of the worst case does not say much about *typical* solvability. For example, the subset of instance of (1) where A is positive semi-definite ($A \succeq 0$) is approximable within constant $\frac{2}{\pi}$ factor [47]. Things even more dramatically change as one gets to random mediums. For (indefinite) A comprised of standard normals (1) becomes famous Sherrington-Kirkpatrick (SK) model [65] where simple

*e-mail: flatoyer@gmail.com

spectral methods ensure (probabilistic) approximability within a constant factor thereby strongly improving over the above mentioned $\log(n)^{\text{const.}}$ inapproximability. Moreover, recent studies [46, 82] move things much further and effectively uncover determining SK-models ground state energies as easy problems.

Following into the footsteps of [82] we here consider *positive* and *negative* Hopfield (\pm Hop) models whose ground state energies are obtained for positive and negative semi-definite forms A . As SK models, Hopfield models have comparably long history [13, 15, 18, 33, 34, 61, 62, 64, 71, 77, 80, 88, 90–92]. Starting out as concepts of cognitive learning [33, 34] they quickly became integral parts of studies in many different areas including physics and mathematics [13, 15, 18, 34, 39, 61, 62, 64, 71, 80, 88, 90–92], statistics, signal processing, algorithmic computer science [16, 17, 19, 44, 47, 67–69, 72, 73], and most notably neural networks [5, 6, 27, 33, 34, 39–43, 48, 61, 63, 81]. Almost all of these applications directly relate to various forms of \pm Hop models ground state energies and impose finding ways to efficiently compute them as a rather pressing need.

Motivated by the success of the *Controlled Loosening-up* (CLuP) algorithms in handling so-called *planted* models in compressed sensing, statistical regression, and MIMO ML detections [72, 73], [82] proposed CLuP-SK counterpart for handling *non-planted* SK models. Building up on [82], we here propose a CLuP \pm Hop alternative for \pm Hop models. Somewhat paradoxically, keeping in mind that [72, 73]’s applications are actually of the (negative) Hopfield type, we in a way reconnect CLuP back to its origin. However, this reconnection is now way more challenging as *non-planted* scenarios are algorithmically much harder. Before we switch to technical intricacies that shed more light on this, we briefly introduce needed mathematical basics and overview some of the most relevant prior results.

2 Hopfield (\pm Hop) models — basics, prior work, and contributions

Form in (1) is a special case of a general statistical mechanics concept. For matrix of quenched interactions G , consider the so-called Hamiltonian

$$\mathcal{H}(G) = \sum_{i=1}^n \sum_{j=1}^m G_{ij} \mathbf{x}_i \mathbf{y}_j = \mathbf{y}^T G \mathbf{x}, \quad (3)$$

and for the *inverse temperature* parameter $\beta > 0$ and the m -dimensional unit norm sphere \mathbb{S}^m associate to it the following partition function

$$Z(\beta, G) = \sum_{\mathbf{x} \in \mathbb{B}^n} \left(\sum_{\mathbf{y} \in \mathbb{S}^m} e^{\beta \mathcal{H}(G)} \right)^s. \quad (4)$$

Throughout the paper we are interested in random $\mathcal{H}(G)$ with elements of G being independent standard normals. We consider so-called linear/proportional regimes with $\alpha = \lim_{n \rightarrow \infty} \frac{m}{n}$ remaining constant as n grows. One then has for the thermodynamic limit ($n \rightarrow \infty$) (average) free energy

$$f_{sq}(\beta) = \lim_{n \rightarrow \infty} \frac{\mathbb{E}_G \log(Z(\beta, G))}{\beta \sqrt{n}} = \lim_{n \rightarrow \infty} \frac{\mathbb{E}_G \log \left(\sum_{\mathbf{x} \in \mathbb{B}^n} \left(\sum_{\mathbf{y} \in \mathbb{S}^m} e^{\beta \mathcal{H}(G)} \right)^s \right)}{\beta \sqrt{n}}, \quad (5)$$

with \mathbb{E}_G standing for the expectation with respect to G (as a general notational convention, subscripts of \mathbb{E} denote the randomness for which the expectation is evaluated). Equipped with all the technicalities we can now introduce the ground state free energy as the following zero-temperature, $\beta \rightarrow \infty$, thermodynamic limit

$$\begin{aligned} f_{sq}(\infty) &\triangleq \lim_{\beta \rightarrow \infty} f_{sq}(\beta) = \lim_{\beta, n \rightarrow \infty} \frac{\mathbb{E}_G \log(Z(\beta, G))}{\beta \sqrt{n}} = \lim_{n \rightarrow \infty} \frac{\mathbb{E}_G \max_{\mathbf{x} \in \mathbb{B}^n} s \max_{\mathbf{y} \in \mathbb{S}^m} \mathcal{H}(G)}{\sqrt{n}} \\ &= \lim_{n \rightarrow \infty} \frac{\mathbb{E}_G \max_{\mathbf{x} \in \mathbb{B}^n} s \max_{\mathbf{y} \in \mathbb{S}^m} \mathbf{y}^T G \mathbf{x}}{\sqrt{n}}. \end{aligned} \quad (6)$$

In particular, we have for $s = 1$

$$\begin{aligned} f_{sq}^+(\infty) &= \lim_{n \rightarrow \infty} \frac{\mathbb{E}_G \max_{\mathbf{x} \in \mathbb{B}^n} \max_{\mathbf{y} \in \mathbb{S}^n} \mathcal{H}(G)}{\sqrt{n}} = \lim_{n \rightarrow \infty} \frac{\mathbb{E}_G \max_{\mathbf{x} \in \mathbb{B}^n} \max_{\mathbf{x} \in \mathbb{S}^m} \mathbf{y}^T G \mathbf{x}}{\sqrt{n}} \\ &= \lim_{n \rightarrow \infty} \frac{\mathbb{E}_G \max_{\mathbf{x} \in \mathbb{B}^n} \sqrt{\mathbf{x}^T G^T G \mathbf{x}}}{\sqrt{n}}, \end{aligned} \quad (7)$$

and for $s = -1$

$$\begin{aligned} f_{sq}^-(\infty) &= \lim_{n \rightarrow \infty} \frac{\mathbb{E}_G \max_{\mathbf{x} \in \mathbb{B}^n} - \max_{\mathbf{y} \in \mathbb{S}^n} \mathcal{H}(G)}{\sqrt{n}} = \lim_{n \rightarrow \infty} \frac{\mathbb{E}_G \max_{\mathbf{x} \in \mathbb{B}^n} - \max_{\mathbf{x} \in \mathbb{S}^m} \mathbf{y}^T G \mathbf{x}}{\sqrt{n}} \\ &= \lim_{n \rightarrow \infty} \frac{\mathbb{E}_G \max_{\mathbf{x} \in \mathbb{B}^n} - \sqrt{\mathbf{x}^T G^T G \mathbf{x}}}{\sqrt{n}} = - \lim_{n \rightarrow \infty} \frac{\mathbb{E}_G \min_{\mathbf{x} \in \mathbb{B}^n} \sqrt{\mathbf{x}^T G^T G \mathbf{x}}}{\sqrt{n}}. \end{aligned} \quad (8)$$

It is now not that difficult to see that (7) is computationally equivalent to (1) with $A = G^T G$ being positive semi-definite. Analogously, (8) is computationally equivalent to (1) with $A = -G^T G$ being negative semi-definite. As precisely such forms of A correspond to *positive* and *negative* Hopfield (\pm Hop) models, the ground state regime and the associated free energies from (7) and (8) are our main focus. However, we find working with the general free energy form from (5) as more convenient. Eventually the ground state \pm Hop's behaviors are deduced as special ($\beta \rightarrow \infty$) cases of (5).

2.1 Prior work

Theoretical aspects: Two spin-glass models – the Edwards-Anderson (EW) nearest neighbor [26] and Sherrington-Kirkpatrick (SK) long range antipode [65] – proposed in the mid seventies of the last century to a large degree shaped up studies in statistical mechanics and many associated computational and engineering fields over the last 50 years. Analysis of the models via [26]’s replica method uncovered incredibly rich intrinsic structures. While it was clear that something big is around the corner, a few unpleasant logical inconsistencies appeared as well. First [65] observed the so-called negative entropy crisis and then extensive followup simulations [38] further uncovered a non-negligible disagreement between the algorithmically computed and theoretically predicted ground state free energies. Attempting to resolve the mismatches, Parisi in a breakthrough discovery [56–58] proposed replacing [26]’s *replica-symmetry* (RS) ansatz with a more refined *replica symmetry breaking* (RSB) one. He demonstrated that already after applying RSB with two steps of breaking, the negative entropy crisis almost completely disappears. Moreover, recognizing that RSB corrections are more pronounced as β grows he also found that two steps of RSB lower the RS ground state energy prediction ≈ 0.7979 to ≈ 0.7636 thereby achieving a stronger agreement with $\sim 0.75 \pm 0.01$ estimate from [38]. Belief in the Parisi RSB quickly strengthened and soon after the appearance of [56–59] it became an irreplaceable tool in utilization of replica methods. While horizons of applications widened, rigorous analytical justifications lagged behind. About 25 years later, Guerra [32] and Talagrand [89] proved that Parisi RSB characterization of the SK model is correct. Panchenko [52–55] reproved these results and additionally established the validity of the *ultrametricity* [59] (for further studies in these and related directions, see, e.g., [8, 9, 36] and references therein).

While all of the above settled the theoretical aspects of the SK models, extensions to more complex models have been noticeably absent. In fact, not only are they not straightforward, but different methodologies are actually needed. Hopfield models are excellent examples where this can be seen. After their invention within cognitive learning context [33, 34], they have been connected to spin glass models [60] and extensively studied within neural networks (NN) communities. Introductory considerations [34, 43] were followed by [6, 20, 66] where free energies were studied for general β ’s via replica methods (some of the problems studied within NN context are actually even more general than the form in (1)). Early mathematical treatments [13, 14, 62, 64, 88, 92] were typically restricted to favorable dimensional and high-temperature (T) regimes (low $\beta = \frac{1}{T}$), where the so-called replica symmetric behavior is present. Outside such regimes, the problems are hard and precise studies were usually replaced by bounding efforts [40–42, 48, 88]. Completely opposite of the high-temperature regime, the ground state assumes zero temperature. Consequently, related available results are even scarcer. Relying on the random duality (RDT) theory, [70] upper bounded the free energy

and showed that such upper bounds precisely match the RS based predictions [23]. Utilizing a *lifted* RDT variant, [71] lowered bounds of [70] and showed that RS predictions are *not* tight implying that symmetry has to be broken. Moreover, for +Hop [71] produced analogous lower bounds, effectively giving the ranges $f_{sq}^+(\infty) \in [1.7632, 1.7832]$ and $f_{sq}^-(\infty) \leq -0.3202$. Finally, fully lifted RDT [78] allowed precise evaluation of \pm Hop ground state free energies. In particular, on the 3rd level of lifting, [80] obtained $f_{sq}^{+,3}(\infty) \approx 1.7789$ and $f_{sq}^{-,3}(\infty) \approx -0.3279$ (in Section 3.2.2 of this paper, we obtain on the 6th level of lifting $f_{sq}^{+,6}(\infty) \approx 1.77842$ and $f_{sq}^{-,6}(\infty) \approx -0.32807$).

Algorithmic aspects: After determining \pm Hop models theoretical limits the natural algorithmic followup question is whether spin configurations that achieve such limits can be efficiently found. As mentioned earlier, within classical NP complexity theory for an indefinite A the optimum in (1) is hard to approximate within a $\log(n)^{const.}$ factor [7]. On the other hand, for any $A \succeq 0$, semi-definite programming (SDP) relaxations ensure constant factor $\frac{2}{\pi}$ approximation [47]. As NP concepts are *worst case* based they rarely give a proper assessment regarding *typical* solvability. A more faithful representation in that regard is obtained after one switches to random mediums (this also happens to be a natural setup of \pm Hop models). In such context, [70] obtained that a simple rounding leading eigenvector procedure gives $f_{sq}^+(\infty) = 2\sqrt{\frac{2}{\pi}}$.

Combining this with a trivial leading eigenvalue bound $f_{sq}^+(\infty) \leq 2$ gives $f_{sq}^+(\infty) \in \left\{\sqrt{\frac{8}{\pi}}, 2\right\}$. Somewhat paradoxically, one obtains the approximating factor of $\frac{2}{\pi}$ (it is actually $\sqrt{\frac{2}{\pi}}$ since $f_{sq}^+(\infty)$ is the root of the optimum in (1) for $A \succeq 0$). In other words simple spectral considerations from [70] give exactly the same approximating factor in random context that [47] gives in non-random. As further hinted in [70], the given range $f_{sq}(\infty) \in \left\{\sqrt{\frac{8}{\pi}}, 2\right\}$ is fairly pessimistic. In fact, another simple iterative procedure presented in [70] gave similar guarantees but practically performed much better producing $f_{sq}^+(\infty) \approx 1.70$ which is much closer to $f_{sq}^+(\infty) \approx 1.7784$. On the other hand, analogous procedure for $-$ Hop model gave $f_{sq}^-(\infty) \approx -0.55$ which is far away from $f_{sq}^-(\infty) \approx -0.3281$. While all of the above put a strong effort in improving the constant factor approximation, it still left one wonder if the approximating factor can approach 1? Or in other words, whether or not the Hopfield models exhibit *computational gaps*? If the approximative factor can be arbitrarily close to 1, then \pm Hop models have no computational gaps and are typically easy (for more on similar phenomena, where problems hard within classical NP theory are actually typically easy, see, e.g., [28–31] and references therein).

We should also mention a few groundbreaking recent results related to similar statistical mechanics models. A continuous random energy model (CREM) was considered in [2] and shown to be solvable in polynomial time. The problem/model is somewhat artificial but it is of great use as it is presumed sufficiently similar to SK when it comes to studying algorithmic properties. Subag in [86] studied p -spin spherical models (also closely related to SK) and designed an efficient algorithm to solve them. Partially inspired by [86], Montanari in [46] provided analogous breakthrough for SK model itself. Differently from [86], [46] relied on modifications of the message passing algorithms [24, 25, 37]. Starting with famous approximate message passing (AMP) [24], [46] considers its an incremental variant, IAMP. and shows that it can compute arbitrarily closely SK ground state energy provided that the Parisi RSB parametric functional is monotonically increasing (or equivalently that the overlap gap property (OGP) is absent [1, 22, 28–31, 45]). Despite missing the formal proofs, these properties are commonly believed to be true (for further extensions in these and closely related directions see also [3, 4, 35, 84, 85, 87]). It would be very interesting to see if the results from [46] (and [86]) can be extended to Hopfield models of interest here.

Following the success of *Control Loosening-up* (CLuP) algorithms in planted models in statistics and signal processing [72, 73], [82] introduced a CLuP-SK algorithm tailored for non-planted SK models. Its practical performance was shown to closely match corresponding theoretical predictions. Moreover, already for the dimensions on the order of few thousands it achieves ~ 76 SK model ground state energy which remarkably closely approaches the thermodynamic $n \rightarrow \infty$ limit of ≈ 0.7632 .

2.2 Our contributions

Given that CLuP-SK [82] provided a nice non-planted model complement for original planted models applications [72, 73], it is natural to wonder if the range of non-planted scenarios solvable by CLuP like algorithms can be further extended. Focusing on Hopfield models as another class of non-planted models, we propose

the following implementation particularly tailored for them

$$\begin{aligned} \text{CLuP}\pm\text{Hop algorithm:} \quad \mathbf{x}^{(t+1)} &\rightarrow \mathbf{gradbar} \left(\bar{f}_{b,x}^{\pm} \left(\mathbf{x}; \bar{t}_{0x}^{(t)} \right); \mathbf{x}^{(t)}, \bar{t}_{0x}^{(t)} \right) \\ \bar{t}_{0x}^{(t+1)} &\rightarrow \bar{c}^{(t)} \bar{t}_{0x}^{(t)}. \end{aligned} \quad (9)$$

For starting $\mathbf{x}^{(t)}$, procedure $\mathbf{gradbar} \left(\bar{f}_{b,x}^+ \left(\mathbf{x}; \bar{t}_{0x}^{(t)} \right); \mathbf{x}^{(t)}, \bar{t}_{0x}^{(t)} \right)$ applies gradient descent to function

$$\bar{f}_{b,x}^+ \left(\mathbf{x}; \bar{t}_{0x}^{(t)} \right) = -\bar{t}_{0x}^{(t)} \|\mathbf{x}\|_2 - \log \left(- \left(\mathbf{x}^T \left(4I - \frac{1}{n} G^T G \right) \mathbf{x} - \kappa \right) \right) - \frac{1}{n} \sum_{i=1}^n \log(1 - n\mathbf{x}_i^2), \quad (10)$$

whereas $\mathbf{gradbar} \left(\bar{f}_{b,x}^- \left(\mathbf{x}; \bar{t}_{0x}^{(t)} \right); \mathbf{x}^{(t)}, \bar{t}_{0x}^{(t)} \right)$ applies gradient descent to function

$$\bar{f}_{b,x}^- \left(\mathbf{x}; \bar{t}_{0x}^{(t)} \right) = -\bar{t}_{0x}^{(t)} \|\mathbf{x}\|_2 - \log \left(- \left(\mathbf{x}^T \left(0I + \frac{1}{n} G^T G \right) \mathbf{x} - \kappa \right) \right) - \frac{1}{n} \sum_{i=1}^n \log(1 - n\mathbf{x}_i^2). \quad (11)$$

Clearly, $\bar{f}_{b,x}^+ \left(\mathbf{x}; \bar{t}_{0x}^{(t)} \right)$ relates to +Hop and $\bar{f}_{b,x}^- \left(\mathbf{x}; \bar{t}_{0x}^{(t)} \right)$ to -Hop model. Also, we found that the above procedure is not overly sensitive to changes of free parameter κ . Choosing $\kappa = 0.855$ for +Hop and $\kappa = 0.115$ for -Hop worked well in all our numerical experiments. Other parameters are also fairly flexible. For example, $t_{0x}^{(0)} = 0.1$ for +Hop and $t_{0x}^{(0)} = 0.001$ for -Hop together with $c^{(t)} = 1.1$ are good starting options that can be adapted as n changes. $\mathbf{x}^{(0)}$ is practically any \mathbf{x} admissible under logs. Taking a random point from $\left\{ -\frac{1}{\sqrt{n}}, \frac{1}{\sqrt{n}} \right\}^n$ and then scaling down by two until a feasible point is reached is a possible choice. Various stopping criteria can be used as well. One option is to take $\bar{t}_{0x}^{(t+1)} \geq 10^4$.

Let $\hat{\mathbf{x}}$ be the output of CLuP \pm Hop. Set

$$\hat{\xi} \triangleq \frac{\mathbb{E}_G \sqrt{\text{sign}(\mathbf{x})^T G^T G \text{sign}(\mathbf{x})}}{n}. \quad (12)$$

Table 1 shows the obtained results for $\hat{\xi}$ for both positive and negative Hopfield models. As can be seen even for n as small as a few thousands one fairly closely approaches the thermodynamic $n \rightarrow \infty$ limits ≈ 1.7784 and ≈ 0.3281 . It should also be noted that the results in the table are obtained for plain gradient descent without any restarts. In other words, they are obtained without any advanced modifications (say, stochastic gradient descent, multiple restarts with carefully chosen restarting points, interactive $t_{0x}^{(0)} = 0.1$ and $c^{(t)}$ retuning, and so on). The effects of such modifications are likely to fade away as $n \rightarrow \infty$, but for finite n they could be beneficial. Since the results shown in Table 1 are already significantly surpassing the best of the expectations, we found no point in overwhelming presentation with extensive discussions regarding additional modifications.

Table 1: Performance of CLuP \pm Hop algorithm; **simulated**/theory

n	2000	4000	8000	∞ (theory)
$\hat{\xi}$ (+Hop)	1.7704	1.7721	1.7735	1.7784
$\hat{\xi}$ (-Hop)	0.3355	0.3340	0.3330	0.3281

To study properties of the above algorithm, we fix r_x ($0 < r_x \leq 1$) and $\bar{r}_x < 0$, and introduce the following

$$\text{CLuP}\pm\text{Hop model:} \quad \max_{\mathbf{x} \in \mathcal{X}(r_x, \bar{r}_x)} \pm \sqrt{\mathbf{x}^T G^T G \mathbf{x}}, \quad (13)$$

with

$$\mathcal{X}(r_x, \bar{r}_x) \triangleq \left\{ \mathbf{x} | \mathbf{x} \in \mathbb{R}^n, \|\mathbf{x}\|_2 = r_x, \mathbf{x}_i^2 \leq \frac{1}{n}, \frac{1}{n} \sum_{i=1}^n \log(1 - n\mathbf{x}_i^2) = \bar{r}_x \right\}. \quad (14)$$

After writing corresponding Hamiltonian and partition function

$$\mathcal{H}_{chop}(G) = \mathbf{y}^T G \mathbf{x}, \quad (15)$$

and

$$Z_{chop}(\beta, G) = \sum_{\mathbf{x} \in \mathcal{X}(r_x, \bar{r}_x)} \left(\sum_{\mathbf{y} \in \mathbb{S}^m} e^{\beta \mathcal{H}_{chop}(G)} \right)^s, \quad (16)$$

we have for the thermodynamic limit (average) free energy

$$f_{chop}(\beta) = \lim_{n \rightarrow \infty} \frac{\mathbb{E}_G \log(Z_{chop}(\beta, G))}{\beta \sqrt{n}} = \lim_{n \rightarrow \infty} \frac{\mathbb{E}_G \log \left(\sum_{\mathbf{x} \in \mathcal{X}(r_x, \bar{r}_x)} \left(\sum_{\mathbf{y} \in \mathbb{S}^m} e^{\beta \mathcal{H}_{chop}(G)} \right)^s \right)}{\beta \sqrt{n}}. \quad (17)$$

For the ground state one then writes

$$\begin{aligned} \xi(r_x, \bar{r}_x) \triangleq f_{chop}(\infty) &\triangleq \lim_{\beta \rightarrow \infty} f_{chop}(\beta) = \lim_{\beta, n \rightarrow \infty} \frac{\mathbb{E}_G \log(Z_{chop}(\beta, G))}{\beta \sqrt{n}} \\ &= \lim_{n \rightarrow \infty} \frac{\mathbb{E}_G \max_{\mathbf{x} \in \mathcal{X}(r_x, \bar{r}_x)} s \max_{\mathbf{y} \in \mathbb{S}^m} \mathcal{H}_{chop}(G)}{\sqrt{n}} \\ &= \lim_{n \rightarrow \infty} \frac{\mathbb{E}_G \max_{\mathbf{x} \in \mathcal{X}(r_x, \bar{r}_x)} s \max_{\mathbf{y} \in \mathbb{S}^m} \mathbf{y}^T G \mathbf{x}}{\sqrt{n}}. \end{aligned} \quad (18)$$

Specializing further to $s = 1$ gives

$$f_{chop}^+(\beta) = \lim_{n \rightarrow \infty} \frac{\mathbb{E}_G \log \left(\sum_{\mathbf{x} \in \mathcal{X}(r_x, \bar{r}_x)} \left(\sum_{\mathbf{y} \in \mathbb{S}^m} e^{\beta \mathcal{H}_{chop}(G)} \right) \right)}{\beta \sqrt{n}}, \quad (19)$$

and

$$\xi^+(r_x, \bar{r}_x) \triangleq f_{chop}^+(\infty) = \lim_{n \rightarrow \infty} \frac{\mathbb{E}_G \max_{\mathbf{x} \in \mathcal{X}(r_x, \bar{r}_x)} \max_{\mathbf{y} \in \mathbb{S}^m} \mathbf{y}^T G \mathbf{x}}{\sqrt{n}} = \lim_{n \rightarrow \infty} \frac{\mathbb{E}_G \max_{\mathbf{x} \in \mathcal{X}(r_x, \bar{r}_x)} \sqrt{\mathbf{x}^T G^T G \mathbf{x}}}{\sqrt{n}}. \quad (20)$$

Analogously for $s = -1$

$$f_{chop}^-(\beta) = \lim_{n \rightarrow \infty} \frac{\mathbb{E}_G \log \left(\sum_{\mathbf{x} \in \mathcal{X}(r_x, \bar{r}_x)} \left(\sum_{\mathbf{y} \in \mathbb{S}^m} e^{\beta \mathcal{H}_{chop}(G)} \right)^{-1} \right)}{\beta \sqrt{n}}, \quad (21)$$

and

$$\begin{aligned} \xi^-(r_x, \bar{r}_x) \triangleq f_{chop}^-(\infty) &= \lim_{n \rightarrow \infty} \frac{\mathbb{E}_G \max_{\mathbf{x} \in \mathcal{X}(r_x, \bar{r}_x)} - \max_{\mathbf{y} \in \mathbb{S}^m} \mathbf{y}^T G \mathbf{x}}{\sqrt{n}} \\ &= \lim_{n \rightarrow \infty} \frac{\mathbb{E}_G \max_{\mathbf{x} \in \mathcal{X}(r_x, \bar{r}_x)} - \sqrt{\mathbf{x}^T G^T G \mathbf{x}}}{\sqrt{n}} = - \lim_{n \rightarrow \infty} \frac{\mathbb{E}_G \min_{\mathbf{x} \in \mathcal{X}(r_x, \bar{r}_x)} \sqrt{\mathbf{x}^T G^T G \mathbf{x}}}{\sqrt{n}}. \end{aligned} \quad (22)$$

Recalling on (10) and (11), one then recognizes that for a fixed t_{0x} of key interest for +Hop is the behavior

of

$$\bar{f}_b^+(r_x, \bar{r}_x) = \min_{\mathbf{x} \in \mathcal{X}(r_x, \bar{r}_x)} -t_{0x} \|\mathbf{x}\|_2 - \log \left(- \left(\mathbf{x}^T \left(4I - \frac{1}{n} G^T G \right) \mathbf{x} - \kappa \right) \right) - \frac{1}{n} \sum_{i=1}^n \log (1 - n \mathbf{x}_i^2), \quad (23)$$

and for $-$ Hop the behavior of

$$\bar{f}_b^-(r_x, \bar{r}_x) = \min_{\mathbf{x} \in \mathcal{X}(r_x, \bar{r}_x)} -t_{0x} \|\mathbf{x}\|_2 - \log \left(- \left(\mathbf{x}^T \left(0I + \frac{1}{n} G^T G \right) \mathbf{x} - \kappa \right) \right) - \frac{1}{n} \sum_{i=1}^n \log (1 - n \mathbf{x}_i^2). \quad (24)$$

Utilizing (13), (20), and (22) we then also have

$$\begin{aligned} \bar{f}_b^+(r_x, \bar{r}_x) &= \min_{\mathbf{x} \in \mathcal{X}(r_x, \bar{r}_x)} -t_{0x} r_x - \log \left(-4r_x^2 + (\bar{\xi}^+(r_x, \bar{r}_x))^2 + \kappa \right) - \bar{r}_x \\ &= -t_{0x} r_x - \log \left(-4r_x^2 + \left(f_{chop}^+(\infty) \right)^2 + \kappa \right) - \bar{r}_x. \end{aligned} \quad (25)$$

and

$$\begin{aligned} \bar{f}_b^-(r_x, \bar{r}_x) &= \min_{\mathbf{x} \in \mathcal{X}(r_x, \bar{r}_x)} -t_{0x} r_x - \log \left(-0r_x^2 + (\bar{\xi}^-(r_x, \bar{r}_x))^2 + \kappa \right) - \bar{r}_x \\ &= -t_{0x} r_x - \log \left(-0r_x^2 + \left(f_{chop}^-(\infty) \right)^2 + \kappa \right) - \bar{r}_x. \end{aligned} \quad (26)$$

The analysis of CLuP \pm Hop algorithm therefore critically depends on $f_{chop}(\infty)$ (i.e., its specialized forms $f_{chop}^+(\infty)$ and $f_{chop}^-(\infty)$). One then quickly recognizes that, in order to properly understand behavior of CLuP \pm Hop algorithm, properties of the associated CLuP \pm Hop models need to be fully understood as well. On the path to achieving that we establish a plethora of results that are of independent interest as well.

- We first connect the CLuP \pm Hop models to recent studies of random processes [74, 77] (see introductory part of Section 3).
- Relying on *fully lifted* random duality theory (fl RDT) and its a *stationarized* sfl RDT variant [78], we then provide concrete characterizations of all relevant CLuP \pm Hop models features (see Sections 3.1 and 3.2).
- Such characterizations are connected with the CLuP \pm Hop algorithms in Section 3.2.1. The algorithms' dynamics are followed through the change of three key features – optimal \bar{f}_b , ξ , and r_x . This is highlighted in Figures 1-3.
- We observe that \bar{f}_b (as a function of r_x) exhibits a favorable no local optima behavior which is a necessary condition for generically successful running of descending algorithms (see Figure 7).
- Due to remarkably rapid convergence of the fl RDT, a majority of quantities of interest are usually sufficiently precisely characterized already on the second or third level of lifting. One notable exception is characterization of configurational overlaps associated Gibbs measures cdfs. To get anywhere close to their true forms significantly higher levels of lifting need to be considered. Along the same lines, we undertake evaluations up to the 6th level and obtain cdfs that simulations closely approach (see Figures 8 and 9 and Tables 3 and 4).
- We uncover a fundamental intrinsic difference between $+$ Hop and $-$ Hop models. Typical near optimal configurations overlaps are well aligned for $+$ Hop and almost orthogonal for $-$ Hop model (see Figures 8 and 9).
- The very same 6th level evaluations allow to obtain $f_{sq}^{+,6}(\infty) \approx 1.77842$ and $f_{sq}^{-,6}(\infty) \approx -0.32807$ as \pm Hop model ground state free energies (see Tables 3 and 4).

- To get a better understanding as to how features of $\pm\text{Hop}$ and SK models compare to each other, in Table 5 and Figure 10 we show the progress of the SK lifting mechanism up to the 7th level. We observe that overlaps of the SK model behave differently from $-\text{Hop}$ model and fairly similarly to $+\text{Hop}$. Interestingly, the SK overlap cdf seems to be higher than the simple approximation given in [51]. On the other hand, we obtain $f_{sq}^{(7)}(\infty) \approx 0.76319$ as the SK model ground state free energy on the 7th lifting level. This indicates that 0.76321 ± 0.00003 prediction of [21] and ≈ 0.76317 prediction of [49, 50] are indeed close to the true value.
- We also practically run CLuP $\pm\text{Hop}$ and show that its simulated performance matches remarkably well obtained theoretical predictions. In particular, we observe excellent convergence and concentration properties (see Figures 1-6). Finally, as Table 1 shows, for n as small as few thousands CLuP $\pm\text{Hop}$ practically achieves $\pm\text{Hop}$ ground state free energies ~ 1.774 and ~ 0.333 , which very closely approaches corresponding $n \rightarrow \infty$ thermodynamic limits ≈ 1.7784 and ≈ 0.3281 . For all practical purposes this basically renders computation of $\pm\text{Hop}$ models ground state free energies as *typically* easy problems.

3 Connecting CLuP $\pm\text{Hop}$ model and sfl RDT

We first note that

$$f_{chop}(\beta) = \lim_{n \rightarrow \infty} \frac{\mathbb{E}_G \log \left(\sum_{\mathbf{x} \in \mathcal{X}(r_x, \bar{r}_x)} \left(\sum_{\mathbf{y} \in \mathbb{S}^m} e^{\beta \mathbf{y}^T G \mathbf{x}} \right)^s \right)}{\beta \sqrt{n}} \quad (27)$$

is a function of bilinearly indexed random process (blirp) $\mathbf{y}^T G \mathbf{x}$. Given that the machinery of [74, 77] provides powerful blirps comparative mechanisms, we would like to connect $f_{chop}(\beta)$ to it. In order to establish such a connection several technical preliminaries are needed. For fixed positive real scalar r_x and \bar{r}_x , consider sets $\mathcal{X}(r_x, \bar{r}_x) \subseteq \mathbb{R}^n$ and $\mathcal{Y} \triangleq \mathbb{S}^m$ (with \mathbb{S}^m be the unit sphere in \mathbb{R}^m). Let $f_S(\cdot) : \mathbb{R}^n \rightarrow \mathbb{R}$ be a given function and for $r \in \mathbb{N}$, $k \in \{1, 2, \dots, r+1\}$ let vectors $\mathbf{p} = [\mathbf{p}_0, \mathbf{p}_1, \dots, \mathbf{p}_{r+1}]$, $\mathbf{q} = [\mathbf{q}_0, \mathbf{q}_1, \dots, \mathbf{q}_{r+1}]$, and $\mathbf{c} = [\mathbf{c}_0, \mathbf{c}_1, \dots, \mathbf{c}_{r+1}]$ be such that

$$\begin{aligned} 1 = \mathbf{p}_0 \geq \mathbf{p}_1 \geq \mathbf{p}_2 \geq \dots \geq \mathbf{p}_r \geq \mathbf{p}_{r+1} &= 0 \\ 1 = \mathbf{q}_0 \geq \mathbf{q}_1 \geq \mathbf{q}_2 \geq \dots \geq \mathbf{q}_r \geq \mathbf{q}_{r+1} &= 0, \end{aligned} \quad (28)$$

$\mathbf{c}_0 = 1$, $\mathbf{c}_{r+1} = 0$. Also let the elements of $u^{(4,k)} \in \mathbb{R}$, $\mathbf{u}^{(2,k)} \in \mathbb{R}^m$, and $\mathbf{h}^{(k)} \in \mathbb{R}^n$ be independent standard normals and set $\mathcal{U}_k \triangleq [u^{(4,k)}, \mathbf{u}^{(2,k)}, \mathbf{h}^{(k)}]$. Moreover, set

$$\psi_{S,\infty}(f_S, \mathcal{X}, \mathcal{Y}, \mathbf{p}, \mathbf{q}, \mathbf{c}, r_x, \bar{r}_x) \triangleq \mathbb{E}_{G, \mathcal{U}_{r+1}} \frac{1}{n \mathbf{c}_r} \log \left(\mathbb{E}_{\mathcal{U}_r} \left(\dots \left(\mathbb{E}_{\mathcal{U}_2} \left(\left(\mathbb{E}_{\mathcal{U}_1} \left((Z_{S,\infty})^{\mathbf{c}_2} \right)^{\frac{\mathbf{c}_3}{\mathbf{c}_2}} \right) \right)^{\frac{\mathbf{c}_4}{\mathbf{c}_3}} \dots \right)^{\frac{\mathbf{c}_r}{\mathbf{c}_{r-1}}} \right), \quad (29)$$

with

$$\begin{aligned} Z_{S,\infty} &\triangleq e^{D_{0,S,\infty}} \\ D_{0,S,\infty} &\triangleq \max_{\mathbf{x} \in \mathcal{X}, \|\mathbf{x}\|_2 = r_x} s \max_{\mathbf{y} \in \mathcal{Y}, \|\mathbf{y}\|_2 = \bar{r}_x} \left(f_S + \sqrt{n} r_y \left(\sum_{k=2}^{r+1} c_k \mathbf{h}^{(k)} \right)^T \mathbf{x} + \sqrt{n} r_x \mathbf{y}^T \left(\sum_{k=2}^{r+1} b_k \mathbf{u}^{(2,k)} \right) \right) \\ b_k &\triangleq b_k(\mathbf{p}) = \sqrt{\mathbf{p}_{k-1} - \mathbf{p}_k} \\ c_k &\triangleq c_k(\mathbf{q}) = \sqrt{\mathbf{q}_{k-1} - \mathbf{q}_k}. \end{aligned} \quad (30)$$

The following theorem is a fundamental sfl RDT result.

Theorem 1 ([78]). *Assume linear/proportional large n regime where $\alpha = \lim_{n \rightarrow \infty} \frac{m}{n}$, remains constant as n grows. Let the elements of $G \in \mathbb{R}^{m \times n}$ be independent standard normals and assume the complete sfl RDT frame from [74]. For three given positive real scalars r_x , \bar{r}_x , and r_y let $\mathcal{X}(r_x, \bar{r}_x) \in \mathbb{R}^n$ and $\mathcal{Y} \in \mathbb{R}^m$ be two*

sets with norm of their elements being r_x and r_y , respectively. For a given function $f(\mathbf{x}) : \mathbb{R}^n \rightarrow \mathbb{R}$ set

$$\begin{aligned}\psi_{rp}(r_x, \bar{r}_x) &\triangleq - \max_{\mathbf{x} \in \mathcal{X}(r_x, \bar{r}_x)} s \max_{\mathbf{y} \in \mathcal{Y}} (f(\mathbf{x}) + \mathbf{y}^T G \mathbf{x}) \quad (\text{random primal}) \\ \psi_{rd}(\mathbf{p}, \mathbf{q}, \mathbf{c}, r_x, \bar{r}_x) &\triangleq \frac{r_x^2 r_y^2}{2} \sum_{k=2}^{r+1} \left(\mathbf{p}_{k-1} \mathbf{q}_{k-1} - \mathbf{p}_k \mathbf{q}_k \right) \mathbf{c}_k \\ &\quad - \psi_{S,\infty}(f(\mathbf{x}), \mathcal{X}(r_x, \bar{r}_x), \mathcal{Y}, \mathbf{p}, \mathbf{q}, \mathbf{c}, r_x, \bar{r}_x) \quad (\text{fl random dual}).\end{aligned}\quad (31)$$

Let $\hat{\mathbf{p}}_0 \rightarrow 1, \hat{\mathbf{q}}_0 \rightarrow 1, \hat{\mathbf{c}}_0 \rightarrow 1, \hat{\mathbf{p}}_{r+1} = \hat{\mathbf{q}}_{r+1} = \hat{\mathbf{c}}_{r+1} = 0$, and let the non-fixed parts of $\hat{\mathbf{p}} \triangleq \hat{\mathbf{p}}(r_x, \bar{r}_x, r_y)$, $\hat{\mathbf{q}} \triangleq \hat{\mathbf{q}}(r_x, \bar{r}_x, r_y)$, and $\hat{\mathbf{c}} \triangleq \hat{\mathbf{c}}(r_x, \bar{r}_x, r_y)$ be the solutions of the following system

$$\frac{d\psi_{rd}(\mathbf{p}, \mathbf{q}, \mathbf{c}, r_x, \bar{r}_x)}{d\mathbf{p}} = 0, \quad \frac{d\psi_{rd}(\mathbf{p}, \mathbf{q}, \mathbf{c}, r_x, \bar{r}_x)}{d\mathbf{q}} = 0, \quad \frac{d\psi_{rd}(\mathbf{p}, \mathbf{q}, \mathbf{c}, r_x, \bar{r}_x)}{d\mathbf{c}} = 0. \quad (32)$$

Then,

$$\lim_{n \rightarrow \infty} \frac{\mathbb{E}_G \psi_{rp}}{\sqrt{n}} = \lim_{n \rightarrow \infty} \psi_{rd}(\hat{\mathbf{p}}(r_x, \bar{r}_x, r_y), \hat{\mathbf{q}}(r_x, \bar{r}_x, r_y), \hat{\mathbf{c}}(r_x, \bar{r}_x, r_y), r_x) \quad (\text{strong sfl random duality}), \quad (33)$$

where $\psi_{S,\infty}(\cdot)$ is as in (29)-(30).

Proof. Follows immediately from [74, 78] after trivial cosmetic changes in the definition of set \mathcal{X} . \square

3.1 Practical relevance

To make use of the above theorem, we take $f(\mathbf{x}) = 0$, $\mathcal{Y} = \mathbb{S}^m$ (with \mathbb{S}^m being the unit sphere in \mathbb{R}^m), and assume that $\mathcal{X}(r_x, \bar{r}_x)$ is as given in (14). Noting that $r_y = 1$ we then recognize that the key object of practical interest is the following so-called *random dual*

$$\begin{aligned}\psi_{rd}(\mathbf{p}, \mathbf{q}, \mathbf{c}, r_x, \bar{r}_x) &\triangleq \frac{r_x^2}{2} \sum_{k=2}^{r+1} \left(\mathbf{p}_{k-1} \mathbf{q}_{k-1} - \mathbf{p}_k \mathbf{q}_k \right) \mathbf{c}_k - \psi_{S,\infty}(0, \mathcal{X}(r_x, \bar{r}_x), \mathcal{Y}, \mathbf{p}, \mathbf{q}, \mathbf{c}, r_x). \\ &= \frac{1}{2} \sum_{k=2}^{r+1} \left(\mathbf{p}_{k-1} \mathbf{q}_{k-1} - \mathbf{p}_k \mathbf{q}_k \right) \mathbf{c}_k - \frac{1}{n} \varphi(D^{(bin)}(r_x, \bar{r}_x)) - \frac{1}{n} \varphi(D^{(sph)}(r_x, \bar{r}_x)),\end{aligned}\quad (34)$$

where analogously to (29)-(30)

$$\varphi(D, \mathbf{c}) = \mathbb{E}_{G, \mathcal{U}_{r+1}} \frac{1}{\mathbf{c}_r} \log \left(\mathbb{E}_{\mathcal{U}_r} \left(\dots \left(\mathbb{E}_{\mathcal{U}_3} \left(\left(\mathbb{E}_{\mathcal{U}_2} \left((e^D)^{\mathbf{c}_2} \right)^{\frac{\mathbf{c}_3}{\mathbf{c}_2}} \right)^{\frac{\mathbf{c}_4}{\mathbf{c}_3}} \dots \right)^{\frac{\mathbf{c}_r}{\mathbf{c}_{r-1}}} \right) \right), \quad (35)$$

and

$$\begin{aligned}D^{(bin)}(r_x, \bar{r}_x) &= \max_{\mathbf{x} \in \mathcal{X}(r_x, \bar{r}_x)} \left(s \sqrt{n} r_y \left(\sum_{k=2}^{r+1} c_k \mathbf{h}^{(k)} \right)^T \mathbf{x} \right) = \max_{\mathbf{x} \in \mathcal{X}(r_x, \bar{r}_x)} \left(s \sqrt{n} \left(\sum_{k=2}^{r+1} c_k \mathbf{h}^{(k)} \right)^T \mathbf{x} \right) \\ D^{(sph)}(r_x, \bar{r}_x) &= s \max_{\mathbf{y} \in \mathcal{Y}} \left(\sqrt{n} r_x \mathbf{y}^T \left(\sum_{k=2}^{r+1} b_k \mathbf{u}^{(2,k)} \right) \right) = s r_x \max_{\mathbf{y} \in \mathbb{S}^m} \left(\sqrt{n} \mathbf{y}^T \left(\sum_{k=2}^{r+1} b_k \mathbf{u}^{(2,k)} \right) \right).\end{aligned}\quad (36)$$

From [82]'s (75) and (76) one finds

$$D^{(bin)}(r_x, \bar{r}_x) = \max_{\mathbf{x} \in \mathcal{X}(r_x, \bar{r}_x)} \left(s \sqrt{n} \left(\sum_{k=2}^{r+1} c_k \mathbf{h}^{(k)} \right)^T \mathbf{x} \right) = \min_{\gamma, \nu} \left(- \sum_{i=1}^n D_i^{(bin)}(c_k) + \gamma r_x^2 n + \nu \bar{r}_x n \right), \quad (37)$$

where scaling $\gamma \sim \gamma\sqrt{n}$ and $\nu \sim \nu\sqrt{n}$ is adopted and

$$D_i^{(bin)}(c_k) = -s \left(\sum_{k=2}^{r+1} c_k \mathbf{h}_i^{(k)} \right) \mathbf{x}_i + \gamma \mathbf{x}_i^2 + \nu \log(1 - n \mathbf{x}_i^2). \quad (38)$$

On the other hand, from [80]'s (29)-(30), we have

$$D^{(sph)}(r_x, \bar{r}_x) = s r_x \min_{\gamma_{sq}} \left(\sum_{i=1}^m D_i^{(sph)}(b_k) + \gamma_{sq} n \right), \quad (39)$$

with

$$D_i^{(sph)}(b_k) = \frac{\left(\sum_{k=2}^{r+1} b_k \mathbf{u}_i^{(2,k)} \right)^2}{4\gamma_{sq}}. \quad (40)$$

After connecting $\xi(r_x, \bar{r}_x)$ and $f_{chop}(\infty)$ from (18) and random primal, $\psi_{rp}(r_x, \bar{r}_x)$, from Theorem 1, we write

$$\begin{aligned} \xi(r_x, \bar{r}_x) = f_{chop}(\infty) &= \lim_{n \rightarrow \infty} \frac{\mathbb{E}_G \max_{\mathbf{x} \in \mathcal{X}(r_x, \bar{r}_x)} s \max_{\mathbf{y} \in \mathbb{S}^m} \mathbf{y}^T G \mathbf{x}}{\sqrt{n}} \\ &= - \lim_{n \rightarrow \infty} \frac{\mathbb{E}_G \psi_{rp}}{\sqrt{n}} = - \lim_{n \rightarrow \infty} \psi_{rd}(\hat{\mathbf{p}}, \hat{\mathbf{q}}, \hat{\mathbf{c}}, r_x, \bar{r}_x), \end{aligned} \quad (41)$$

where the non-fixed parts of $\hat{\mathbf{p}}$, $\hat{\mathbf{q}}$, and $\hat{\mathbf{c}}$ satisfy

$$\frac{d\psi_{rd}(\mathbf{p}, \mathbf{q}, \mathbf{c}, r_x, \bar{r}_x)}{d\mathbf{p}} = 0, \quad \frac{d\psi_{rd}(\mathbf{p}, \mathbf{q}, \mathbf{c}, r_x, \bar{r}_x)}{d\mathbf{q}} = 0, \quad \frac{d\psi_{rd}(\mathbf{p}, \mathbf{q}, \mathbf{c}, r_x, \bar{r}_x)}{d\mathbf{c}} = 0. \quad (42)$$

Relying on (34)-(42), we further have

$$\lim_{n \rightarrow \infty} \psi_{rd}(\hat{\mathbf{p}}, \hat{\mathbf{q}}, \hat{\mathbf{c}}, r_x, \bar{r}_x) = \bar{\psi}_{rd}(\hat{\mathbf{p}}, \hat{\mathbf{q}}, \hat{\mathbf{c}}, \hat{\gamma}, \hat{\nu}, \hat{\gamma}_{sq}, r_x, \bar{r}_x), \quad (43)$$

where

$$\begin{aligned} \bar{\psi}_{rd}(\mathbf{p}, \mathbf{q}, \mathbf{c}, \gamma, \nu, \gamma_{sq}, r_x, \bar{r}_x) &= \frac{1}{2} \sum_{k=2}^{r+1} \left(\mathbf{p}_{k-1} \mathbf{q}_{k-1} - \mathbf{p}_k \mathbf{q}_k \right) \mathbf{c}_k - \gamma r_x^2 - \nu \bar{r}_x - \varphi(D_1^{(bin)}(c_k(\mathbf{q})), \mathbf{c}) \\ &\quad - s \gamma_{sq} r_x - \alpha \varphi(D_1^{(sph)}(b_k(\mathbf{p})), \mathbf{c}). \end{aligned} \quad (44)$$

Based on (35), (38), and (40), $\varphi(D_1^{(bin)}(c_k(\mathbf{q})), \mathbf{c})$ and $\varphi(D_1^{(sph)}(b_k(\mathbf{p})), \mathbf{c})$ in (44) are given by

$$\begin{aligned} \varphi(D_1^{(bin)}(c_k(\mathbf{q})), \mathbf{c}) &= \mathbb{E}_{\mathcal{U}_{r+1}} \frac{1}{\mathbf{c}_r} \log \left(\mathbb{E}_{\mathcal{U}_r} \left(\dots \left(\mathbb{E}_{\mathcal{U}_3} \left(\left(\mathbb{E}_{\mathcal{U}_2} \left(e^{-\mathbf{c}_2 D_1^{(bin)}(c_k(\mathbf{q}))} \right)^{\frac{\mathbf{c}_3}{\mathbf{c}_2}} \right) \right)^{\frac{\mathbf{c}_4}{\mathbf{c}_3}} \dots \right)^{\frac{\mathbf{c}_r}{\mathbf{c}_{r-1}}} \right), \\ \varphi(D_1^{(sph)}(b_k(\mathbf{p})), \mathbf{c}) &= \mathbb{E}_{\mathcal{U}_{r+1}} \frac{1}{\mathbf{c}_r} \log \left(\mathbb{E}_{\mathcal{U}_r} \left(\dots \left(\mathbb{E}_{\mathcal{U}_3} \left(\left(\mathbb{E}_{\mathcal{U}_2} \left(e^{s r_x \mathbf{c}_2 D_1^{(sph)}(b_k(\mathbf{p}))} \right)^{\frac{\mathbf{c}_3}{\mathbf{c}_2}} \right) \right)^{\frac{\mathbf{c}_4}{\mathbf{c}_3}} \dots \right)^{\frac{\mathbf{c}_r}{\mathbf{c}_{r-1}}} \right), \end{aligned} \quad (45)$$

whereas $\hat{\gamma}$, $\hat{\nu}$, $\hat{\gamma}_{sq}$, and the non-fixed parts of $\hat{\mathbf{p}}$, $\hat{\mathbf{q}}$, and $\hat{\mathbf{c}}$ are the solutions of

$$\begin{aligned} \frac{d\bar{\psi}_{rd}(\mathbf{p}, \mathbf{q}, \mathbf{c}, \gamma, \nu, \gamma_{sq}, r_x, \bar{r}_x)}{d\mathbf{p}} &= \frac{d\bar{\psi}_{rd}(\mathbf{p}, \mathbf{q}, \mathbf{c}, \gamma, \nu, \gamma_{sq}, r_x, \bar{r}_x)}{d\mathbf{q}} = \frac{d\bar{\psi}_{rd}(\mathbf{p}, \mathbf{q}, \mathbf{c}, \gamma, \nu, \gamma_{sq}, r_x, \bar{r}_x)}{d\mathbf{c}} = 0 \\ \frac{d\bar{\psi}_{rd}(\mathbf{p}, \mathbf{q}, \mathbf{c}, \gamma, \nu, \gamma_{sq}, r_x, \bar{r}_x)}{d\gamma} &= \frac{d\bar{\psi}_{rd}(\mathbf{p}, \mathbf{q}, \mathbf{c}, \gamma, \nu, \gamma_{sq}, r_x, \bar{r}_x)}{d\nu} = \frac{d\bar{\psi}_{rd}(\mathbf{p}, \mathbf{q}, \mathbf{c}, \gamma, \nu, \gamma_{sq}, r_x, \bar{r}_x)}{d\gamma_{sq}} = 0. \end{aligned}$$

(46)

After observing

$$\begin{aligned} b_k(\hat{\mathbf{p}}) &= \sqrt{\hat{\mathbf{p}}_{k-1} - \hat{\mathbf{p}}_k} \\ c_k(\hat{\mathbf{q}}) &= \sqrt{\hat{\mathbf{q}}_{k-1} - \hat{\mathbf{q}}_k}, \end{aligned} \quad (47)$$

and connecting (41) to (43) one further finds

$$\begin{aligned} f_{chop}(\infty) &= \lim_{n \rightarrow \infty} \frac{\mathbb{E}_G \max_{\mathbf{x} \in \mathcal{X}(r_x, \bar{r}_x)} s \max_{\mathbf{t} \in \mathbb{S}^m} \mathbf{y}^T G \mathbf{x}}{\sqrt{n}} \\ &= - \lim_{n \rightarrow \infty} \psi_{rd}(\hat{\mathbf{p}}, \hat{\mathbf{q}}, \hat{\mathbf{c}}, r_x, \bar{r}_x) = -\bar{\psi}_{rd}(\hat{\mathbf{p}}, \hat{\mathbf{q}}, \hat{\mathbf{c}}, \hat{\gamma}, \hat{\nu}, \hat{\gamma}_{sq}, r_x, \bar{r}_x) \\ &= -\frac{1}{2} \sum_{k=2}^{r+1} \left(\hat{\mathbf{p}}_{k-1} \hat{\mathbf{q}}_{k-1} - \hat{\mathbf{p}}_k \hat{\mathbf{q}}_k \right) \hat{\mathbf{c}}_k + \hat{\gamma} r_x^2 + \hat{\nu} \bar{r}_x + \varphi(D_1^{(bin)}(c_k(\hat{\mathbf{q}})), \mathbf{c}) \\ &\quad + s \hat{\gamma}_{sq} r_x + \alpha \varphi(D_1^{(sph)}(b_k(\hat{\mathbf{p}})), \mathbf{c}). \end{aligned} \quad (48)$$

We summarize the above results in the following theorem.

Theorem 2. Consider linear/proportional large n regime with $\alpha = \lim_{n \rightarrow \infty} \frac{m}{n}$ and assume the complete sfl RDT setup of [74]. Let the “fixed” parts of $\hat{\mathbf{p}}$, $\hat{\mathbf{q}}$, and $\hat{\mathbf{c}}$ be $\hat{\mathbf{p}}_1 \rightarrow 1$, $\hat{\mathbf{q}}_1 \rightarrow 1$, $\hat{\mathbf{c}}_1 \rightarrow 1$, $\hat{\mathbf{p}}_{r+1} = \hat{\mathbf{q}}_{r+1} = \hat{\mathbf{c}}_{r+1} = 0$. For $\varphi(\cdot)$ and $\bar{\psi}_{rd}(\cdot)$ from (35) and (44) let $\hat{\gamma}$, $\hat{\nu}$, $\hat{\gamma}_{sq}$, and the “non-fixed” parts of $\hat{\mathbf{p}}_k$, $\hat{\mathbf{q}}_k$, and $\hat{\mathbf{c}}_k$ ($k \in \{2, 3, \dots, r\}$) be the solutions of (46). Taking $b_k(\hat{\mathbf{p}})$ and $c_k(\hat{\mathbf{q}})$ as in (47) gives

$$\begin{aligned} \xi(r_x, \bar{r}_x) \triangleq f_{chop}(\infty) &= -\bar{\psi}_{rd}(\hat{\mathbf{p}}, \hat{\mathbf{q}}, \hat{\mathbf{c}}, \hat{\gamma}, \hat{\nu}, \hat{\gamma}_{sq}, r_x, \bar{r}_x) \\ &= -\frac{1}{2} \sum_{k=2}^{r+1} \left(\hat{\mathbf{p}}_{k-1} \hat{\mathbf{q}}_{k-1} - \hat{\mathbf{p}}_k \hat{\mathbf{q}}_k \right) \hat{\mathbf{c}}_k + \hat{\gamma} r_x^2 + \hat{\nu} \bar{r}_x + \varphi(D_1^{(bin)}(c_k(\hat{\mathbf{q}})), \mathbf{c}) \\ &\quad + s \hat{\gamma}_{sq} r_x + \alpha \varphi(D_1^{(sph)}(b_k(\hat{\mathbf{p}})), \mathbf{c}). \end{aligned} \quad (49)$$

Proof. Follows directly from (48) as an immediate consequence of the above discussion and Theorem 1. \square

3.2 Numerical evaluations

Theorem 2 is practically relevant as long as all the underlying numerical evaluations can be conducted. We show next how this is done. It turns out as convenient to work with the third partial level of lifting (we denote it as 3-spl RDT; in general, for the r -th level we follow the convention of [80] and denote partial and full lifting by r -spl and r -sfl, respectively). Such a choice makes a nice balance between accuracy and numerical burden (for example, recalling on [80], one has that on the third partial level the limiting \pm Hop ground state energies are approached with accuracy ~ 0.001).

To put everything on concrete terms, we first note that on the third partial level $r = 3$ and $\hat{\mathbf{p}}_1 \rightarrow 1$, $\hat{\mathbf{q}}_1 \rightarrow 1$, and $\hat{\mathbf{p}}_{r+1} = \hat{\mathbf{p}}_4 = \hat{\mathbf{q}}_{r+1} = \hat{\mathbf{q}}_4 = 0$. In addition to having $\hat{\mathbf{c}}_2 \neq 0$, $\hat{\mathbf{c}}_3 \neq 0$, $\mathbf{p}_2 \neq 0$, and $\mathbf{q}_2 \neq 0$ one also has $\mathbf{p}_3 = \mathbf{q}_3 = 0$. Keeping all of this in mind we can then write

$$\begin{aligned} -\bar{\psi}_{rd}^{(3,p)}(\mathbf{p}, \mathbf{q}, \mathbf{c}, \gamma, \nu, \gamma_{sq}, r_x, \bar{r}_x) &= -\frac{1}{2}(1 - \mathbf{p}_2 \mathbf{q}_2) \mathbf{c}_2 r_x^2 - \frac{1}{2} \mathbf{p}_2 \mathbf{q}_2 \mathbf{c}_3 r_x^2 \\ &\quad + \gamma r_x^2 + \nu \bar{r}_x + \frac{1}{\mathbf{c}_3} \log \left(\mathbb{E}_{\mathcal{U}_3} \left(\mathbb{E}_{\mathcal{U}_2} e^{-\mathbf{c}_2 D_1^{(bin)}(c_k(\mathbf{q}))} \right)^{\frac{\mathbf{c}_3}{\mathbf{c}_2}} \right) \\ &\quad + s \gamma r_x + \frac{\alpha}{\mathbf{c}_3} \log \left(\mathbb{E}_{\mathcal{U}_3} \left(\mathbb{E}_{\mathcal{U}_2} e^{s r_x \mathbf{c}_2 D_1^{(sph)}(b_k(\mathbf{p}))} \right)^{\frac{\mathbf{c}_3}{\mathbf{c}_2}} \right) \\ &= -\frac{1}{2}(1 - \mathbf{p}_2 \mathbf{q}_2) \mathbf{c}_2 r_x^2 - \frac{1}{2} \mathbf{p}_2 \mathbf{q}_2 \mathbf{c}_3 r_x^2 + \gamma r_x^2 + \nu \bar{r}_x + f_q^{(3,p)} + s \gamma_{sq} r_x + \alpha f_{q,s}^{(3,p)}, \end{aligned} \quad (50)$$

where

$$f_q^{(3,p)} = \frac{1}{\mathbf{c}_3} \log \left(\mathbb{E}_{\mathcal{U}_3} \left(\mathbb{E}_{\mathcal{U}_2} e^{-\mathbf{c}_2 D_1^{(bin)}(c_k(\mathbf{q}))} \right)^{\frac{\mathbf{c}_3}{\mathbf{c}_2}} \right), \quad (51)$$

and based on [80]'s (48) and (90)

$$\begin{aligned} f_{q,s}^{(3,p)} &= \frac{\alpha}{\mathbf{c}_3} \log \left(\mathbb{E}_{\mathcal{U}_3} \left(\mathbb{E}_{\mathcal{U}_2} e^{s r_x \mathbf{c}_2 D_1^{(sph)}(b_k(\mathbf{p}))} \right)^{\frac{\mathbf{c}_3}{\mathbf{c}_2}} \right) \\ &= \alpha \left(-\frac{1}{2\mathbf{c}_2} \log \left(\frac{2s\gamma_{sq} - \mathbf{c}_2 r_x (1 - \mathbf{p}_2)}{2s\gamma_{sq}} \right) - \frac{1}{2\mathbf{c}_3} \log \left(\frac{2s\gamma_{sq} - \mathbf{c}_2 r_x (1 - \mathbf{p}_2) - \mathbf{c}_3 r_x \mathbf{p}_2}{2s\gamma_{sq} - \mathbf{c}_2 r_x (1 - \mathbf{p}_2)} \right) \right). \end{aligned} \quad (52)$$

The above provides all necessary ingredients to conduct the concrete numerical evaluations. We show next what results such evaluations produce.

3.2.1 Concrete results

Recalling on (25) and (26) we first write

$$\begin{aligned} \bar{f}_b^+(r_x, \bar{r}_x) &= \min_{\mathbf{x} \in \bar{\mathcal{X}}(r_x, \bar{r}_x)} -t_{0x} r_x - \log \left(-4r_x^2 + (\xi^+(r_x, \bar{r}_x))^2 + \kappa \right) - \bar{r}_x \\ &= -t_{0x} r_x - \log \left(-4r_x^2 + \left(f_{chop}^+(\infty) \right)^2 + \kappa \right) - \bar{r}_x, \end{aligned} \quad (53)$$

and

$$\begin{aligned} \bar{f}_b^-(r_x, \bar{r}_x) &= \min_{\mathbf{x} \in \bar{\mathcal{X}}(r_x, \bar{r}_x)} -t_{0x} r_x - \log \left(-0r_x^2 + (\xi^-(r_x, \bar{r}_x))^2 + \kappa \right) - \bar{r}_x \\ &= -t_{0x} r_x - \log \left(-0r_x^2 + \left(f_{chop}^-(\infty) \right)^2 + \kappa \right) - \bar{r}_x. \end{aligned} \quad (54)$$

After setting

$$\bar{r}_x^{(opt, \pm)} \triangleq \operatorname{argmin}_{\bar{r}_x < 0} \bar{f}_b^\pm(r_x, \bar{r}_x), \quad (55)$$

and

$$\begin{aligned} \bar{f}_b^\pm(r_x) &\triangleq \min_{\bar{r}_x < 0} \bar{f}_b^\pm(r_x, \bar{r}_x) = \bar{f}_b^\pm(r_x, \bar{r}_x^{(opt, \pm)}) \\ \xi^\pm(r_x) &\triangleq \xi^\pm(r_x, \bar{r}_x^{(opt, \pm)}), \end{aligned} \quad (56)$$

we have for the optimal r_x

$$\hat{r}_x^\pm = \operatorname{argmin}_{r_x \in (0, 1]} \bar{f}_b^\pm(r_x). \quad (57)$$

After conducting all numerical evaluations we obtained results presented in Figures 1-3. Theoretical predictions for the dynamics of all three critical quantities, $\frac{\bar{f}_b(\hat{r}_x)}{t_{0x}}$, $\xi(\hat{r}_x)$, and \hat{r}_x are shown (\pm signs are skipped in all figures to lighten notation; clearly for +Hop model, all quantities are with + sign and for -Hop with - sign). Also, for the very same quantities, we in parallel show the simulated results obtained by running CLuP±Hop algorithm for $n = 200$, $n = 1000$, and $n = 4000$. Despite the simulated dimensions being rather small (compared to $n \rightarrow \infty$), an excellent agreement between theoretical and simulated results is observed.

We should also add another interesting point. Namely, all of the above numerical evaluations were repeated while relying on modulo- \mathbf{m} sfl results from [74, 77, 78] with no difference in the obtained results. This indicates the *minimization* type of \mathbf{c} stationarity and is in a remarkable agreement with the same type of discovery from [75, 76, 80, 82, 83].

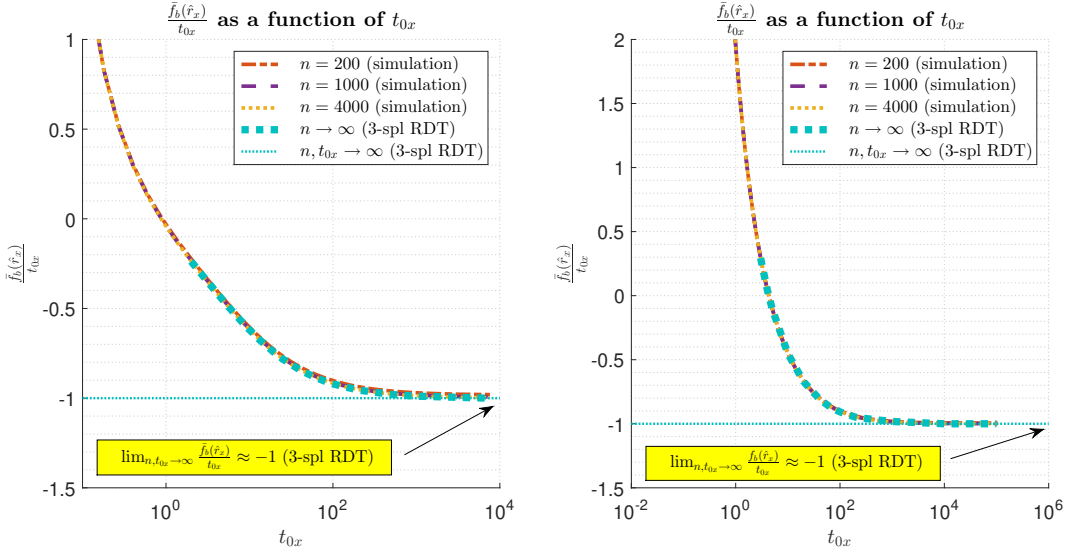


Figure 1: $\frac{\bar{f}_b(\hat{r}_x)}{t_{0x}}$ as a function of t_{0x} ; +Hop (left) and -Hop (right)

3.2.2 Properties

The conducted experiments allowed also to look at several interesting properties in more detail.

Convergence with respect to n

The theoretical results are obtained in the thermodynamic limit with $n \rightarrow \infty$. Since only finite n 's can be simulated, it is interesting to see how quickly simulated results converge as n increases. We focus on key quantity of interest, $\xi(\hat{r}_x)$, and show in Figure 4 how it changes as a function of n . Starting with n as small as a few tens and then increasing it to reach a few thousands we observe the pace at which the simulated CLuP±Hop dynamics approach theoretical predictions. For +Hop the most rapid portion of the convergence process happens for $n \leq 1000$ and then it visibly slows down. On the other hand, for -Hop after starting slowly for $n \sim 100$ and the convergence speeds up for $n \sim 1000$ before naturally slowing down as n gets to the range of several thousands. Such -Hop behavior is somewhat interesting and it should be noted that it is in an excellent agreement with observations made in [70].

In Figure 5 we show how $\lim_{t_{0x} \rightarrow \infty} \xi(\hat{r}_x)$ changes with n ($\lim_{t_{0x} \rightarrow \infty} \xi(\hat{r}_x)$ is the limiting value of $\xi(\hat{r}_x)$ obtained at the end of the algorithm's running). $\lim_{t_{0x} \rightarrow \infty} \hat{\xi}(\hat{r}_x)$ – the effective objective value of (1) produced by the algorithm and an emulation of $\lim_{t_{0x} \rightarrow \infty} \xi(\hat{r}_x)$ obtained after $\pm \frac{1}{\sqrt{n}}$ rounding of the algorithm's output $\hat{\mathbf{x}}$ – is shown in parallel as well. Clearly, for $n \rightarrow \infty$ the two quantities $\lim_{t_{0x} \rightarrow \infty} \xi(\hat{r}_x)$ and $\lim_{t_{0x} \rightarrow \infty} \hat{\xi}(\hat{r}_x)$ are indistinguishable. However, for finite n they do differ and one expects the difference to fade away as n increases. As Figure 5 shows, this indeed happens. Moreover, it happens already for n as small as a few thousands.

Concentrations

Closely related to the above convergence are the concentration properties. Theory predicts that for $n \rightarrow \infty$ all key underlying quantities rapidly concentrate. Figure 6 shows a finite dimensional emulation of concentration effects. In the upper portion of the figure we have +Hop and in the lower portion -Hop concentration results. For both scenarios we have taken $n = 200$ and $m = 4000$ as representatives of smaller and larger n . One observes a rapid onset of concentrations effects with standard deviations dropping 7 – 8 times for the given n span. Moreover, we superimposed Gaussian densities with means and standard deviations that match the ones obtained through simulations. As figure shows, they remarkably well fit the simulated histograms.

Objective shape as a function of r_x

In Figure 7, we show the scaled objective $\frac{\bar{f}_b(r_x)}{t_{0x}}$ for a concrete $t_{0x} = 20$. For both +Hop and -Hop we observe that $\frac{\bar{f}_b(r_x)}{t_{0x}}$ has no local optima. We also repeated the very same test across a wide range of

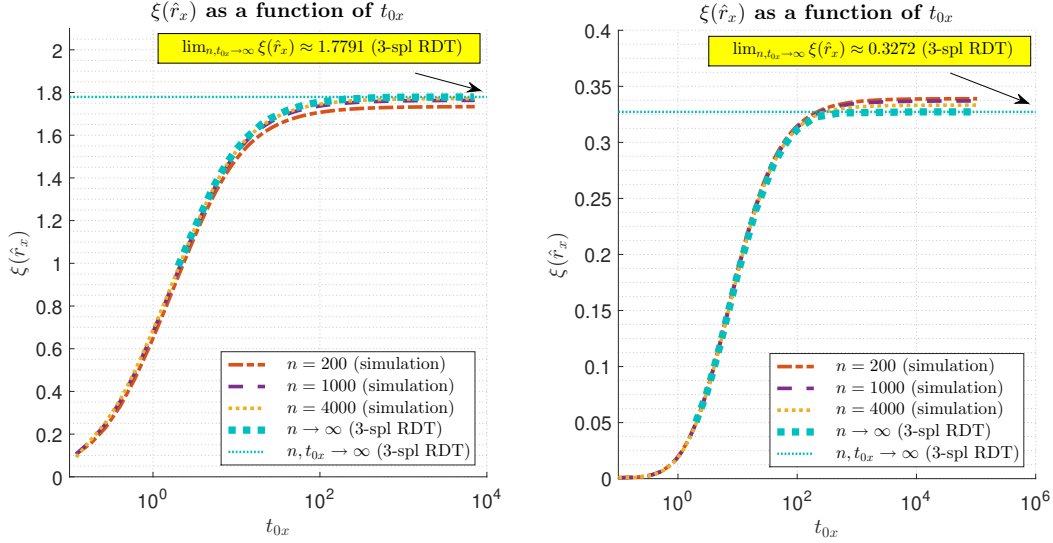


Figure 2: $\bar{\xi}(\hat{r}_x)$ as a function of t_{0x} ; +Hop (left) and -Hop (right)

t_{0x} and observed the same trend. Such an absence of objective’s local optima is a necessary condition for successful generic running of descending algorithms. To what degree (if any) intrinsic features other than objective landscape impact performance of descending algorithms remains to be seen. Studying potential presence/absence of “near optimal” solutions clustering organization might be interesting next steps in these directions. In particular, overlap gap properties (OGP) [1, 22, 28–31, 45] and local entropies (LE) [10–12] are two clustering related concepts predominantly present in recent literature. We should also add that the shape of the objective critically depends on the accuracy of the underlying numerical evaluations. As mentioned earlier, all our evaluations are done on the third partial level of lifting. Tiny corrections do appear on higher lifting levels but remain visually almost undetectable and without significant impact on objective’s shape.

Restarting/retuning

As mentioned earlier, all our results are obtained for basic \pm Hop implementations. Even though the obtained results are well above the best of hopes, significant improvement in certain scenarios can be achieved with fairly minimal modifications/adaptations. For example, just restarting with different randomly chosen initial configurations already helps a lot. Retuning $c^{(t)}$ as the algorithm progresses provides an additional help as well. To give a flavor as to what kind of improvement one can expect, we in Table 2 show the impact of restarting+retuning modification on -Hop (in our experience -Hop seems to benefit the most from additional modifications). We limited number of restarts to 100 (even though 20 was typically sufficient) and retuned $c^{(t)}$ as $c^{(t)} = \text{Unif}[1, 1.3]$. We selected two scenarios $n = 500$ and $n = 2000$ to emphasize that a strong improvement is possible across a range of n including those on the order of few thousands where the theoretical limits are already being approached fairly closely.

Table 2: Restarting/retuning effects on CLuP-Hop algorithm – **plain**/restart+retune

n	500	2000	∞ (theory)
$\hat{\xi}(-\text{Hop})$	0.3430	0.3355	0.3281
$\hat{\xi}(-\text{Hop})$	0.3358	0.3330	0.3281

Overlaps

Excellent CLuP \pm Hop performance allows simulation of near optimal solutions – configurations that produce energies in the vicinity of the optimal ground state one. Of particular interest are the overlaps structures together with associated Gibbs measures. In the thermodynamic limit the key components of the

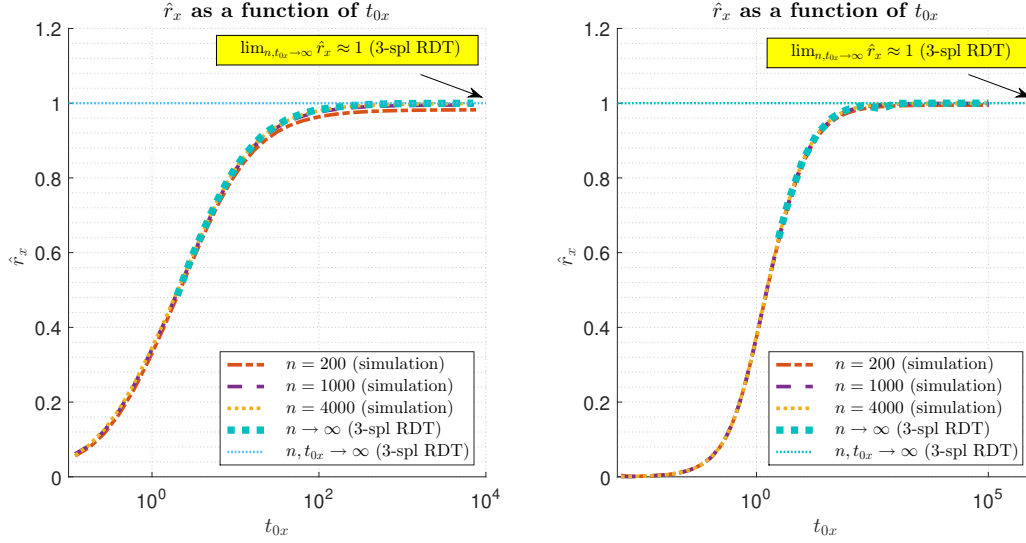


Figure 3: \hat{r}_x as a function of t_{0x} ; +Hop (left) and -Hop (right)

Gibbs measures concentrate on $\mathbf{p}_2, \mathbf{p}_3, \dots, \mathbf{p}_r$ and $\mathbf{q}_2, \mathbf{q}_3, \dots, \mathbf{q}_r$. In Figure 8 and 9 we show how the structure of \mathbf{p} and \mathbf{q} changes as lifting progresses. Visual presentation is somewhat facilitated if one associates with \mathbf{p} , \mathbf{q} , and \mathbf{c} the following

$$\begin{aligned}
 \mathbf{p} \left(\frac{\mathbf{c}}{\mathbf{c}_2} \right) \text{ map:} & \quad \mathbf{p}_2 \leftrightarrow \left[\frac{\mathbf{c}_3}{\mathbf{c}_2}, \frac{\mathbf{c}_2}{\mathbf{c}_2} \right], \quad \mathbf{p}_3 \leftrightarrow \left[\frac{\mathbf{c}_4}{\mathbf{c}_2}, \frac{\mathbf{c}_3}{\mathbf{c}_2} \right], \quad \dots, \\
 \mathbf{q} \left(\frac{\mathbf{c}}{\mathbf{c}_2} \right) \text{ map:} & \quad \mathbf{q}_2 \leftrightarrow \left[\frac{\mathbf{c}_3}{\mathbf{c}_2}, \frac{\mathbf{c}_2}{\mathbf{c}_2} \right], \quad \mathbf{q}_3 \leftrightarrow \left[\frac{\mathbf{c}_4}{\mathbf{c}_2}, \frac{\mathbf{c}_3}{\mathbf{c}_2} \right], \quad \dots,
 \end{aligned} \tag{58}$$

for +Hop model and

$$\begin{aligned}
 \mathbf{p} \left(\frac{\mathbf{c}}{\mathbf{c}_\infty} \right) \text{ map:} & \quad \mathbf{p}_2 \leftrightarrow \left[\frac{\mathbf{c}_2}{\mathbf{c}_\infty}, \frac{\mathbf{c}_3}{\mathbf{c}_\infty} \right], \quad \mathbf{p}_3 \leftrightarrow \left[\frac{\mathbf{c}_3}{\mathbf{c}_\infty}, \frac{\mathbf{c}_4}{\mathbf{c}_\infty} \right], \quad \dots, \\
 \mathbf{q} \left(\frac{\mathbf{c}}{\mathbf{c}_\infty} \right) \text{ map:} & \quad \mathbf{q}_2 \leftrightarrow \left[\frac{\mathbf{c}_2}{\mathbf{c}_\infty}, \frac{\mathbf{c}_3}{\mathbf{c}_\infty} \right], \quad \mathbf{q}_3 \leftrightarrow \left[\frac{\mathbf{c}_3}{\mathbf{c}_\infty}, \frac{\mathbf{c}_4}{\mathbf{c}_\infty} \right], \quad \dots
 \end{aligned} \tag{59}$$

for -Hop model. Concrete numerical values for \mathbf{p} , \mathbf{q} , and \mathbf{c} up to the 6th lifting level are given in Tables 3 and 4 [80] (Table 3 relates to +Hop and Table 4 to +Hop model; in addition to \mathbf{p} , \mathbf{q} , and \mathbf{c} the r th level values of $f_{sq}^+(\infty)$ and $f_{sq}^-(\infty)$, $f_{sq}^{+,r}(\infty)$ and $f_{sq}^{-,r}(\infty)$, are given as well; as stated above, results from the tables are also visualized in Figures 8 and 9). Moreover, $\mathbf{p}(\cdot)$ and $\mathbf{q}(\cdot)$ maps are complemented with simulated near optimal configurations overlaps (we ran randomly restarted algorithm's variant). The simulated distributions fairly closely match the \mathbf{p} and \mathbf{q} Gibbs measures cdfs. Also, comparing Figures 8 and 9 one observes a fundamentally different behavior of +Hop and -Hop overlaps. Both \mathbf{p} and \mathbf{q} +Hop overlaps are typically close to one which means that near optimal solutions \mathbf{x} (as well as their corresponding \mathbf{y} 's) are “*typically close*” to each other. On the other hand, in -Hop model they are “*typically far away*” and usually almost orthogonal to each other. We should add that due to the dependence on the choice of near optimality (we have taken ± 0.003 as allowed deviation from the algorithm's best solution) simulated results are more an indication than accurate value (simulating exact values seems as a conceptually rather hard task).

We complement \pm Hop models overlaps results with the corresponding SK ones. In Table 5 we show the SK lifting progression up to the 7th level. Results from Table 5 are visualized in Figure 10 (since there is a rather large number of numerical evaluations increasing their level of precision might slightly change the 6th and 7th level numbers in Table 5; however, shape and location of the corresponding curves in Figure

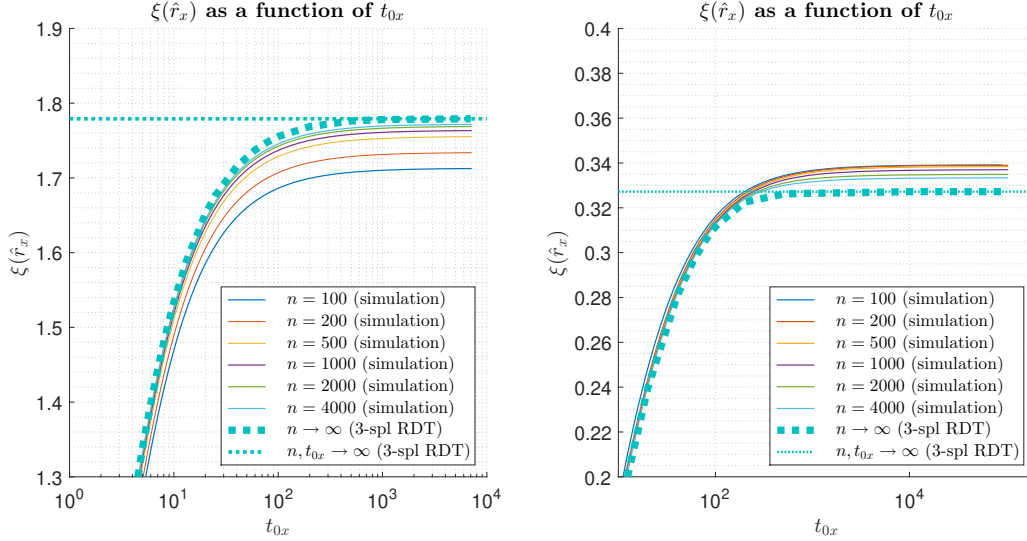


Figure 4: Convergence of $\bar{\xi}(\hat{r}_x)$ as n grows; +Hop (left) and -Hop (right)

10 as well as $f_{csk}^{(r)}$ (the r th level SK ground state free energy) are not expected to significantly change). It is interesting to note that SK overlaps cdf is much more similar to +Hop than to -Hop. Furthermore, the SK overlap cdf seems to be higher than the simple approximation given in [51] (denoted as ∞ -RSB estimate in Figure 10). On the other hand, we obtain $f_{csk}^{(7)}(\infty) \approx 0.76319$ as the SK model ground state free energy on the 7th lifting level. This indicates that 0.76321 ± 0.00003 prediction of [21] and ≈ 0.76317 prediction of [49, 50] are indeed close to the true value. The simulated SK overlap values are shown as well (we ran restarted algorithm's variant together with random deviations in t_{0x}). One should note though, that (compared to \pm Hop) overlaps simulations in SK case seem more sensitive to the choice of near optimality and as such should be taken even more cautiously as an indication of the true behavior. Nonetheless, the trend in the bulk of the distribution is very much in alignment with the theoretical prediction.

4 Conclusion

We studied algorithmic aspects of *positive* and *negative* Hopfield (\pm Hop) models and focused on determining their ground state free energies. These problems are equivalent to binary maximization of random positive/negative semi-definite quadratic forms. Their indefinite quadratic form analogue is the celebrated SK model. Following the success of *Controlled Loosening-up* (CLuP-SK) algorithms in computing near ground state free energies of SK models [82], we here proposed CLuP \pm Hop analogues for \pm Hop models. An excellent performance is observed already for n as small as few thousands. In particular, we have that: (i) CLuP+Hop achieves ~ 1.77 as the ground state free energy of the positive model; and (ii) CLuP-Hop achieves ~ 0.33 as the corresponding energy of the negative model. Both of these closely approach the theoretical thermodynamic ($n \rightarrow \infty$) limits ≈ 1.7784 and ≈ 0.3281 and position computation of near ground state free energies of \pm Hop models as *typically* easy problems.

To analyze the introduced algorithms we associated the CLuP \pm Hop models and utilized Fully lifted random duality theory (fl RDT) [78] to study them. A generic analytical framework was developed and employed to characterize the entire dynamics of the proposed algorithms. Already on the third (partial) level of lifting (3-spl RDT) we obtained almost identical match between the theoretical predictions and algorithmically simulated results. Excellent algorithmic performance and generality of the analytical concepts allowed to uncover a host of interesting features as well. Strong convergence and concentration properties are observed (already for $n \sim 1000$) and a favorable – no local optima – landscape of the underlying algorithmic objective is uncovered.

Lifting up to the 3rd level is usually sufficient to obtain very precise characterizations of almost any

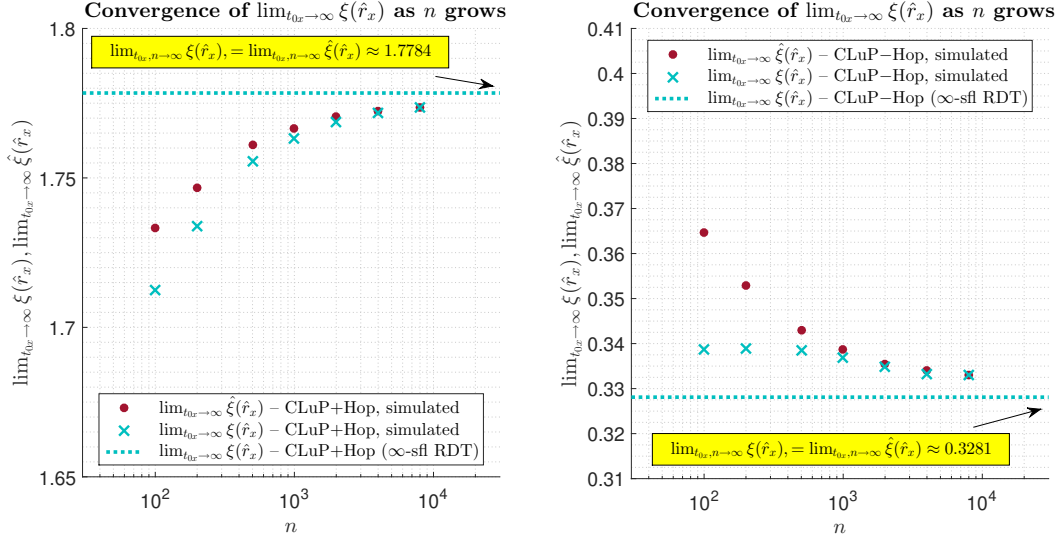


Figure 5: Convergence of $\lim_{t_{0x} \rightarrow \infty} \xi(\hat{r}_x)$ and $\lim_{t_{0x} \rightarrow \infty} \hat{\xi}(\hat{r}_x)$ as n grows; +Hop (left) and -Hop (right)

associated performance measure. One notable exception is the characterization of the configurational overlaps and their Gibbs measures. To handle these much higher levels of lifting are needed. We conducted evaluations up to the 6th lifting level (6-spl RDT) and along the way uncovered a remarkable fundamental intrinsic difference between +Hop and -Hop models. Typical near optimal configurations are *close* to each other for +Hop and *far away* for -Hop model.

The introduced concepts are very generic and allow for many extensions as well. Developing CLuP analogues for various models discussed in [74, 77–79] forms just a small fraction of practically endless possibilities. In addition to relying on the main concepts presented here and in [72, 73, 82], these extensions also require a bit of technical adjustments that are usually problem specific. We discuss these in separate papers.

References

- [1] D. Achlioptas, A. Coja-Oghlan, and F. Ricci-Tersenghi. On the solution-space geometry of random constraint satisfaction problems. *Random Struct. Algorithms*, 38(3):251–268, 2011.
- [2] L. Addario-Berry and P. Maillard. The algorithmic hardness threshold for continuous random energy models. *Math. Stat. Learn.*, 2:77–101, 2019.
- [3] A. E. Alaoui, A. Montanari, and M. Sellke. Sampling from the Sherrington-Kirkpatrick gibbs measure via algorithmic stochastic localization. In *63rd IEEE Annual Symposium on Foundations of Computer Science, FOCS 2022, Denver, CO, USA, October 31 - November 3, 2022*, pages 323–334. IEEE, 2022.
- [4] A. E. Alaoui, A. Montanari, and M. Sellke. Shattering in pure spherical spin glasses. *Communications in Mathematical Physics*, 406(111), 2025.
- [5] D. Amit, H. Gutfreund, and H. Sompolinsky. Statistical mechanics of neural networks. *Annals of Physics*, 173:30–47, 1987.
- [6] D. J. Amit, H. Gutfreund, and H. Sompolinsky. Storing infinite number of patterns in a spin glass model of neural networks. *Phys. Rev. Letters*, 55:1530, 1987.
- [7] S. Arora, E. Berger, E. Hazan, G. Kindler, and M. Safra. On non-approximability for quadratic programs. In *46th Annual IEEE Symposium on Foundations of Computer Science (FOCS 2005), 23-25 October 2005, Pittsburgh, PA, USA, Proceedings*, pages 206–215. IEEE Computer Society, 2005.

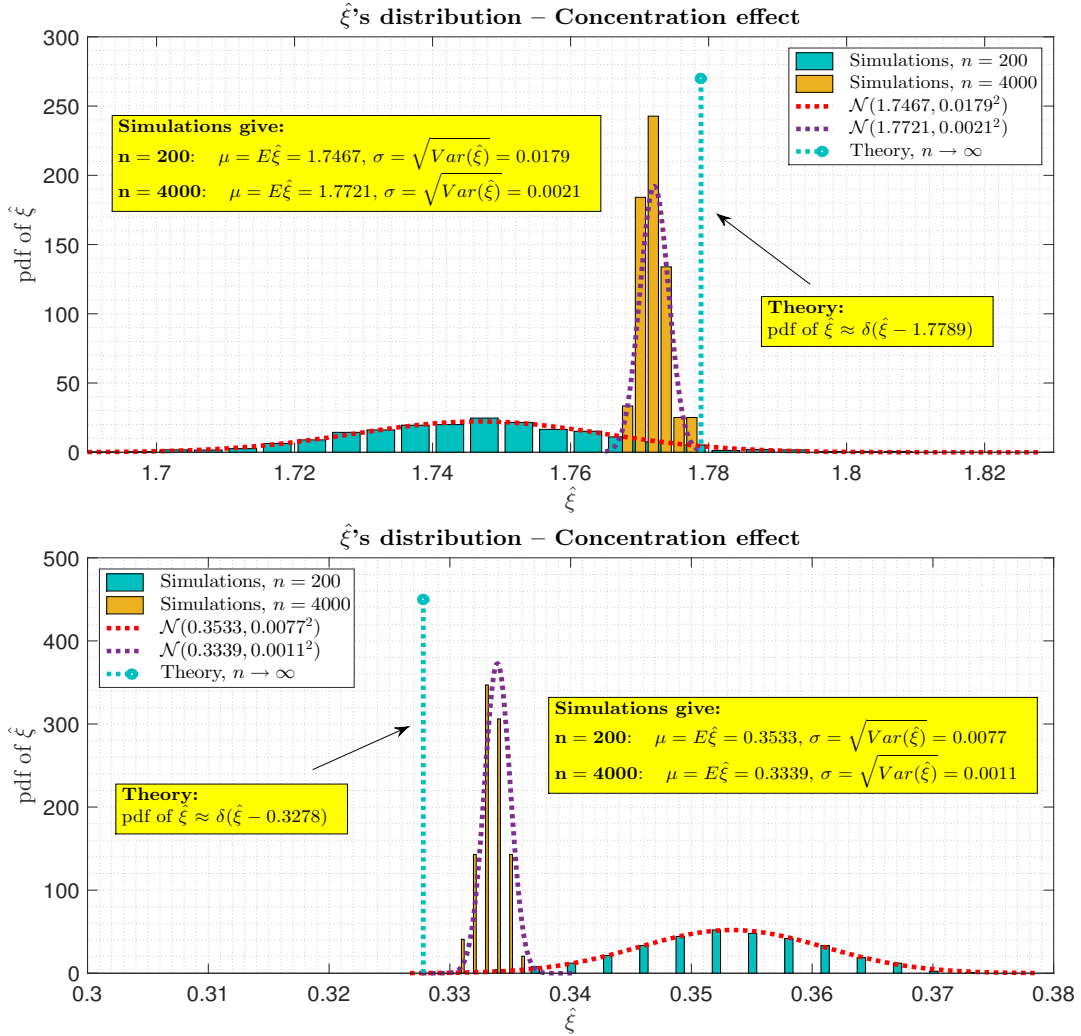


Figure 6: Concentration effect; +Hop (top) and -Hop (bottom)

- [8] A. Auffinger and W.-K. Chen. The Parisi formula has a unique minimizer. *Communications in Mathematical Physics*, 335(3), 2015.
- [9] A. Auffinger, W.-K. Chen, and Q. Zheng. The SK model is infinite step replica symmetry breaking at zero temperature. *Comm. Pure Appl. Math.*, 73, 2020.
- [10] C. Baldassi, A. Ingrosso, C. Lucibello, L. Saglietti, and R. Zecchina. Subdominant dense clusters allow for simple learning and high computational performance in neural networks with discrete synapses. *Physical Review letters*, 115(12):128101, 2015.
- [11] C. Baldassi, A. Ingrosso, C. Lucibello, L. Saglietti, and R. Zecchina. Local entropy as a measure for sampling solutions in constraint satisfaction problems. *Journal of Statistical Mechanics: Theory and Experiment*, (2):021301, 2016.
- [12] C. Baldassi, R. D. Vecchia, C. Lucibello, and R. Zecchina. Clustering of solutions in the symmetric binary perceptron. *Journal of Statistical Mechanics: Theory and Experiment*, (7):073303, 2020.
- [13] A. Barra, G. Genovese, and F. Guerra. The replica symmetric approximation of the analogical neural network. *J. Stat. Physics*, July 2010.

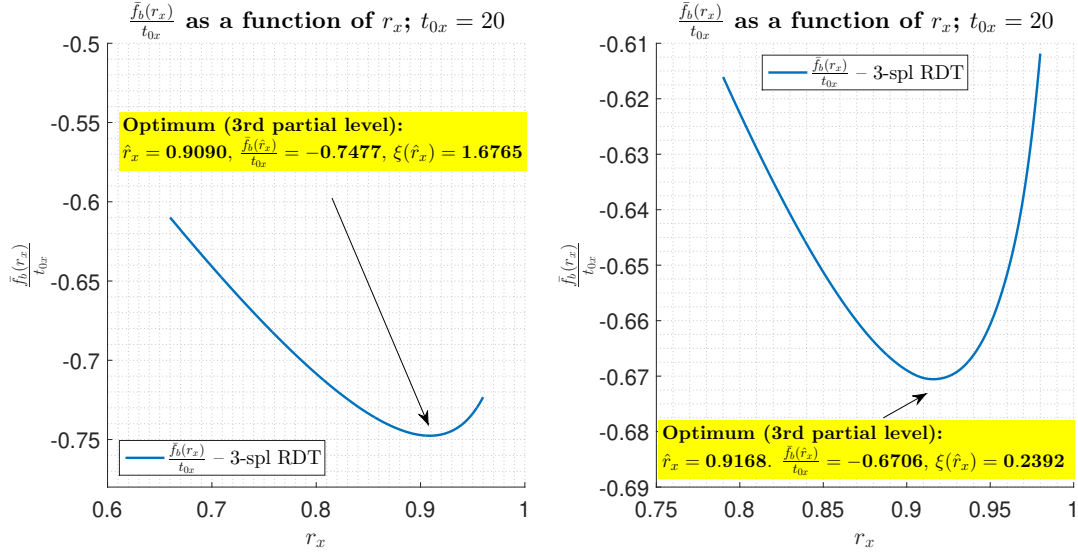


Figure 7: Landscape as a function of r_x ; +Hop (left) and -Hop (right)

- [14] A. Barra, G. Genovese, and F. Guerra. Equilibrium statistical mechanics of bipartite spin systems. *Journal of Physics A: Mathematical and Theoretical*, 44(245002), 2011.
- [15] A. Barra, G. Genovese, F. Guerra, and D. Tantari. How glassy are neural networks. *J. Stat. Mechanics: Theory and Experiment*, July 2012.
- [16] M. Bayati and A. Montanari. The dynamics of message passing on dense graphs, with applications to compressed sensing. *IEEE Trans. Inf. Theory*, 57(2):764–785, 2011.
- [17] M. Bayati and A. Montanari. The LASSO risk for gaussian matrices. *IEEE Trans. Inf. Theory*, 58(4):1997–2017, 2012.
- [18] A. Bovier and V. Gayrard. Hopfield models as generalized random mean field models. In *mathematical aspects of spin glasses and neural networks*, *Progr. Prob.*, 41:3–89, 1998.
- [19] M. Charikar and A. Wirth. Maximizing quadratic programs: Extending grothendieck’s inequality. In *45th Symposium on Foundations of Computer Science (FOCS 2004), 17-19 October 2004, Rome, Italy, Proceedings*, pages 54–60. IEEE Computer Society, 2004.
- [20] A. Crisanti, D. J. Amit, and H. Gutfreund. Saturation level of the Hopfield model for neural network. *Europhys. Lett.*, (2):337, 1986.
- [21] A. Crisanti and T. Rizzo. Analysis of the ∞ -replica symmetry breaking solution of the Sherrington-Kirkpatrick model. *Phys. Rev. E*, 65(4):046137, Apr 2002.
- [22] H. Daude, M. Mezard, T. Mora, and R. Zecchina. Pairs of sat-assignments in random boolean formulae. *Theoretical Computer Science*, 393(1):260–279, 2008.
- [23] D. Dean and F. Ritort. Squared interaction matrix Sherrington-Kirkpatrick model for a spin glass. *Phys. Rev. B*, 65:224209, 2002.
- [24] D. Donoho, A. Maleki, and A. Montanari. Message-passing algorithms for compressed sensing. *Proc. National Academy of Sciences*, 106(45):18914–18919, Nov. 2009.
- [25] D. L. Donoho, A. Maleki, and A. Montanari. The noise-sensitivity phase transition in compressed sensing. *IEEE Trans. Inf. Theory*, 57(10):6920–6941, 2011.

Table 3: r -sfl RDT parameters; +Hop model; $\alpha = 1$; $\hat{\mathbf{c}}_1 \rightarrow 1$; $n, \beta \rightarrow \infty$

r	$\hat{\gamma}_{sq}$	$[\hat{\mathbf{p}}_{r-1} \ \hat{\mathbf{p}}_{r-2} \ \dots \ \hat{\mathbf{p}}_1]^T$	$[\hat{\mathbf{q}}_{r-1} \ \hat{\mathbf{q}}_{r-2} \ \dots \ \hat{\mathbf{q}}_1]^T$	$[\hat{\mathbf{c}}_r \ \hat{\mathbf{c}}_{r-1} \ \dots \ \hat{\mathbf{c}}_2]^T$	$f_{sq}^{+,r}$
2	0.6173	$\begin{bmatrix} \rightarrow 1 \end{bmatrix}$	$\begin{bmatrix} \rightarrow 1 \end{bmatrix}$	$\begin{bmatrix} 0.4246 \end{bmatrix}$	1.7832
3	0.7434	$\begin{bmatrix} 0.7510 \\ \rightarrow 1 \end{bmatrix}$	$\begin{bmatrix} 0.8397 \\ \rightarrow 1 \end{bmatrix}$	$\begin{bmatrix} 0.2508 \\ 1.7762 \end{bmatrix}$	1.7791
4	0.8024	$\begin{bmatrix} 0.5900 \\ 0.9097 \\ \rightarrow 1 \end{bmatrix}$	$\begin{bmatrix} 0.6927 \\ 0.9546 \\ \rightarrow 1 \end{bmatrix}$	$\begin{bmatrix} 0.1829 \\ 0.8349 \\ 3.9792 \end{bmatrix}$	1.77859
5	0.8203	$\begin{bmatrix} 0.4230 \\ 0.97700 \\ 0.9473 \\ \rightarrow 1 \end{bmatrix}$	$\begin{bmatrix} 0.5205 \\ 0.8556 \\ 0.9762 \\ \rightarrow 1 \end{bmatrix}$	$\begin{bmatrix} 0.1214 \\ 0.4705 \\ 1.4078 \\ 5.6138 \end{bmatrix}$	1.77846
6	0.8235	$\begin{bmatrix} 0.3030 \\ 0.6132 \\ 0.8398 \\ 0.9602 \\ \rightarrow 1 \end{bmatrix}$	$\begin{bmatrix} 0.3786 \\ 0.7141 \\ 0.9093 \\ 0.9833 \\ \rightarrow 1 \end{bmatrix}$	$\begin{bmatrix} 0.0883 \\ 0.3041 \\ 0.7092 \\ 1.8885 \\ 6.3850 \end{bmatrix}$	1.77842

- [26] S. F. Edwards and P. W. Anderson. J. phys. f. 5:965, 1975.
- [27] J. Feng, M. Shcherbina, and B. Tirozzi. On the critical capacity of the Hopfield model. *Communications in Mathematical Physics*, 2000.
- [28] D. Gamarnik. The overlap gap property: A topological barrier to optimizing over random structures. *Proceedings of the National Academy of Sciences*, 118(41), 2021.
- [29] D. Gamarnik and M. Sudan. Limits of local algorithms over sparse random graphs. *Proceedings of the 5th conference on innovations in theoretical computer science*, pages 369–376, 2014.
- [30] D. Gamarnik and M. Sudan. Limits of local algorithms over sparse random graphs. *Ann. Probab.*, 45(4):2353–2376, 2017.
- [31] D. Gamarnik and M. Sudan. Performance of sequential local algorithms for the random NAE-K-SAT problem. *SIAM Journal on Computing*, 46(2):590–619, 2017.
- [32] F. Guerra. Broken replica symmetry bounds in the mean field spin glass model. *Comm. Math. Physics*, 233:1–12, 2003.
- [33] D. O. Hebb. Organization of behavior. *New York: Wiley*, 1949.
- [34] J. J. Hopfield. Neural networks and physical systems with emergent collective computational abilities. *Proc. Nat. Acad. Science*, 79:2554, 1982.
- [35] B. Huang and M. Sellke. Tight lipschitz hardness for optimizing mean field spin glasses. In *63rd IEEE Annual Symposium on Foundations of Computer Science, FOCS 2022, Denver, CO, USA, October 31 - November 3, 2022*, pages 312–322. IEEE, 2022.

Table 4: r -sfl RDT parameters; $-\text{Hop}$ model; $\alpha = 1$; $\hat{\mathbf{c}}_1 \rightarrow 1$; $n, \beta \rightarrow \infty$

r	$\hat{\gamma}_{sq}$	$[\hat{\mathbf{p}}_{r-1} \ \hat{\mathbf{p}}_{r-2} \ \dots \ \hat{\mathbf{p}}_1]^T$	$[\hat{\mathbf{q}}_{r-1} \ \hat{\mathbf{q}}_{r-2} \ \dots \ \hat{\mathbf{q}}_1]^T$	$[\hat{\mathbf{c}}_r \ \hat{\mathbf{c}}_{r-1} \ \dots \ \hat{\mathbf{c}}_2]^T$	$f_{sq}^{-,r}$
2	0.1654	$\begin{bmatrix} \rightarrow 1 \end{bmatrix}$	$\begin{bmatrix} \rightarrow 1 \end{bmatrix}$	$\begin{bmatrix} 2.6916 \end{bmatrix}$	0.3202
3	0.1748	$\begin{bmatrix} 0.5722 \\ \rightarrow 1 \end{bmatrix}$	$\begin{bmatrix} 0.0599 \\ \rightarrow 1 \end{bmatrix}$	$\begin{bmatrix} 10.548 \\ 2.2264 \end{bmatrix}$	0.3272
4	0.1766	$\begin{bmatrix} 0.3639 \\ 0.6836 \\ \rightarrow 1 \end{bmatrix}$	$\begin{bmatrix} 0.0107 \\ 0.1282 \\ \rightarrow 1 \end{bmatrix}$	$\begin{bmatrix} 27.9800 \\ 5.0700 \\ 2.1306 \end{bmatrix}$	0.3279
5	0.1776	$\begin{bmatrix} 0.2640 \\ 0.5137 \\ 0.7307 \\ \rightarrow 1 \end{bmatrix}$	$\begin{bmatrix} 0.0035 \\ 0.0387 \\ 0.1742 \\ \rightarrow 1 \end{bmatrix}$	$\begin{bmatrix} 54.3693 \\ 9.3081 \\ 3.7962 \\ 2.1046 \end{bmatrix}$	0.32803
6	0.1774	$\begin{bmatrix} 0.2040 \\ 0.3982 \\ 0.5835 \\ 0.7556 \\ \rightarrow 1 \end{bmatrix}$	$\begin{bmatrix} 0.0016 \\ 0.0148 \\ 0.0648 \\ 0.2036 \\ \rightarrow 1 \end{bmatrix}$	$\begin{bmatrix} 85.9067 \\ 15.8758 \\ 6.2406 \\ 3.2936 \\ 2.0872 \end{bmatrix}$	0.32807

- [36] A. Jagannath and I. Tobasco. A dynamic programming approach to the Parisi functional. In *Proceedings of the American Mathematical Society*, volume 14, pages 3135–3150.
- [37] Y. Kabashima. A CDMA multiuser detection algorithm on the basis of belief propagation. *L. Phys. A*, 36.
- [38] S. Kirkpatrick and D. Sherrington. *Phys. Rev. B*, 17:4384, 1978.
- [39] D. Krotov and J. J. Hopfield. Dense associative memory for pattern recognition. *Advances in Neural Information Processing Systems*, 1:1180–1188, 2016.
- [40] D. Loukianova. Capacite de memoire dans le modele de Hopfield. *C. R. Acad. Sci. Paris t. 318, Serie I*, pages 157–160, 1994.
- [41] D. Loukianova. Etude rigoureuse du modele de Hopfield de memoire associative. *These de doctorat de l'Universite Paris 7*, 1994.
- [42] D. Loukianova. Lower bounds on the restitution error in the Hopfield model. *Probab. Theory Related Fields*, 107:161–176, 1997.
- [43] R. J. MacEliece, E. C. Posner, E. Rodemich, and S.S. Venkatesh. The capacity of the Hopfield associative memory. *IEEE Trans. Inform. Theory*, 33:461–482, 1987.
- [44] A. Megretski. Relaxation of quadratic programs in operator theory and system analysis. In *In Systems, Approximation, Singular Integral Operators, and Related Topics (Bordeaux)*, pages 365–92, 2000.
- [45] M. Mezard, T. Mora, and R. Zecchina. Clustering of solutions in the random satisfiability problem. *Physical Review Letters*, 94:197204, 2005.

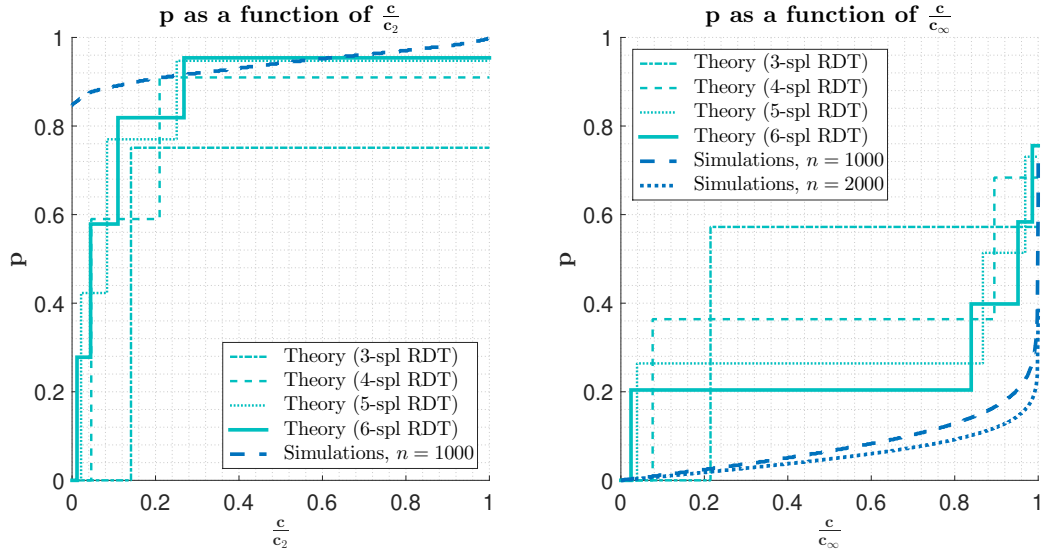


Figure 8: \mathbf{p} overlaps; +Hop (left) and -Hop (right)

Table 5: r -sfl RDT parameters; SK model; $\hat{\mathbf{q}}_1, \hat{\mathbf{c}}_1 \rightarrow 1$; $n, \beta \rightarrow \infty$

r	$\hat{\mathbf{q}}_5$	$\hat{\mathbf{q}}_4$	$\hat{\mathbf{q}}_4$	$\hat{\mathbf{q}}_3$	$\hat{\mathbf{q}}_2$	$\hat{\mathbf{c}}_5$	$\hat{\mathbf{c}}_4$	$\hat{\mathbf{c}}_5$	$\hat{\mathbf{c}}_4$	$\hat{\mathbf{c}}_3$	$\hat{\mathbf{c}}_2$	$f_{csk}^{(r)}(\infty)$
2	0	0	0	0	0	$\rightarrow 0$	$\rightarrow 0$	$\rightarrow 0$	$\rightarrow 0$	$\rightarrow 0$	0.5779	0.76883
3	0	0	0	0	0.7434	$\rightarrow 0$	$\rightarrow 0$	$\rightarrow 0$	$\rightarrow 0$	0.3569	1.4586	0.76403
4	0	0	0	0.5587	0.9088	$\rightarrow 0$	$\rightarrow 0$	$\rightarrow 0$	0.2599	0.8280	2.5103	0.76341
5	0	0	0.4421	0.7912	0.9588	$\rightarrow 0$	$\rightarrow 0$	0.2048	0.6104	1.3026	3.7571	0.76326
6	0	0.3708	0.6952	0.8939	0.9796	$\rightarrow 0$	0.1718	0.5027	0.9485	1.8802	5.3556	0.76321
7	0.2854	0.5363	0.7621	0.9133	0.9829	0.1381	0.3752	0.6383	1.08235	2.0709	5.8472	0.76319

- [46] A. Montanari. Optimization of the Sherrington-Kirkpatrick hamiltonian. In *60th IEEE Annual Symposium on Foundations of Computer Science, FOCS 2019, Baltimore, Maryland, USA, November 9-12, 2019*, pages 1417–1433. IEEE Computer Society, 2019.
- [47] Y. Nesterov. Quality of semidefinite relaxation for nonconvex quadratic optimization. *CORE discussion paper*, 9719, 1997.
- [48] Ch. M. Newman. Memory capacity and neural network models: Rigorous lower bounds. *Neural Networks*, 1:223–238, 1988.
- [49] R. Oppermann and M. J. Schmidt. Universality class of replica symmetry breaking, scaling behavior, and the low-temperature fixed-point order function of the Sherrington-Kirkpatrick model. *Phys. Rev. E*, 78(6):061124, Dec 2008.
- [50] R. Oppermann, M. J. Schmidt, and D. Sherrington. Double criticality of the Sherrington-Kirkpatrick model at $t = 0$. *Phys. Rev. Lett.*, 98(12):127201, Mar 2007.
- [51] R. Oppermann and D. Sherrington. Scaling and renormalization group in replica-symmetry-breaking space: Evidence for a simple analytical solution of the Sherrington-Kirkpatrick model at zero temperature. *Phys. Rev. Lett.*, 95(19):197203, Nov 2005.
- [52] D. Panchenko. A connection between the Ghirlanda-Guerra identities and ultrametricity. *The Annals of Probability*, 38(1):327–347, 2010.

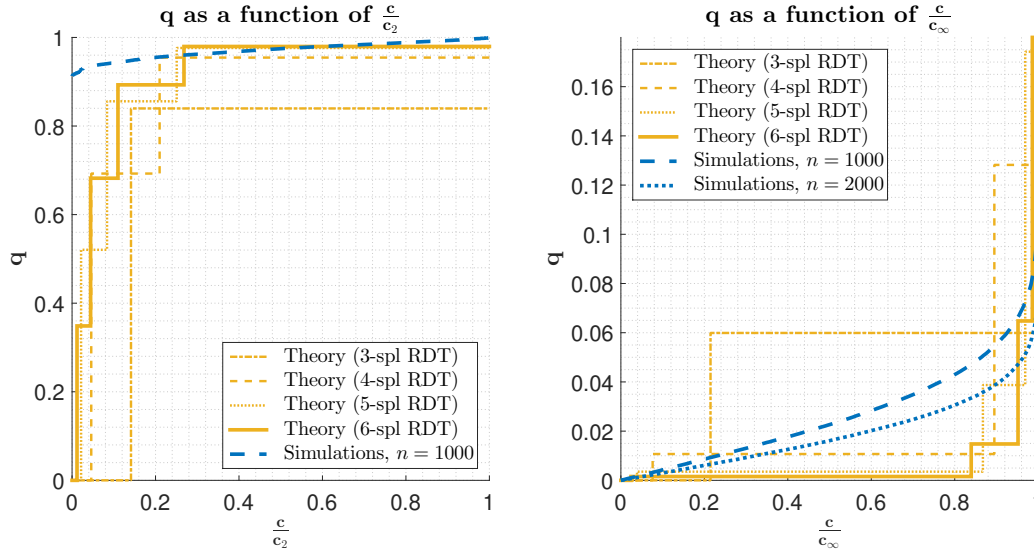


Figure 9: q overlaps; +Hop (left) and -Hop (right)

- [53] D. Panchenko. The Ghirlanda-Guerra identities for mixed p-spin model. *Comptes Rendus Mathematique*, 348(3-4):189–192, 2010.
- [54] D. Panchenko. The Parisi ultrametricity conjecture. *Ann. Math.*, 77(1):383–393, 2013.
- [55] D. Panchenko. *The Sherrington-Kirkpatrick model*. Springer Science & Business Media, 2013.
- [56] G. Parisi. Infinite number of order parameters for spin-glasses. *Phys. Rev. Lett.*, 43:1754–1756, 1979.
- [57] G. Parisi. Breaking the symmetry in SK model. *J. Physics*, A13:1101, 1980.
- [58] G. Parisi. A sequence of approximated solutions to the SK model for spin glasses. *Journal of Physics A: Mathematical and General*, 13(4):L115, 1980.
- [59] G. Parisi. Order parameter for spin glasses. *Phys. Rev. Lett.*, 50:1946, 1983.
- [60] L. Pastur and A. Figotin. Exactly soluble model of a spin-glass. *Soviet J. of Low Temperature Phys.*, 3(378-383), 1977.
- [61] L. Pastur and A. Figotin. On the theory of disordered spin systems. *Theory Math. Phys.*, 35(403-414), 1978.
- [62] L. Pastur, M. Shcherbina, and B. Tirozzi. The replica-symmetric solution without the replica trick for the Hopfield model. *Journal of Statistical Physics*, 74(5/6), 1994.
- [63] H. Ramsauer, B. Schaffl, J. Lehner, P. Seidl, M. Widrich, L. Gruber, M. Holzleitner, T. Adler, D. Kreil, M. K. Kopp, G. Klambauer, J. Brandstetter, and S. Hochreiter. Hopfield networks is all you need. *In International Conference on Learning Representations*, 2021.
- [64] M. Shcherbina and B. Tirozzi. The free energy of a class of Hopfield models. *Journal of Statistical Physics*, 72(1/2), 1993.
- [65] D. Sherrington and S. Kirkpatrick. Solvable model of a spin-glass. *Phys. Rev. Lett.*, 35:1792–1796, Dec 1975.
- [66] H. Steffan and R. Kuhn. Replica symmetry breaking in attractor neural network models. *Z. Phys. B*, 95:249–260, 1994.

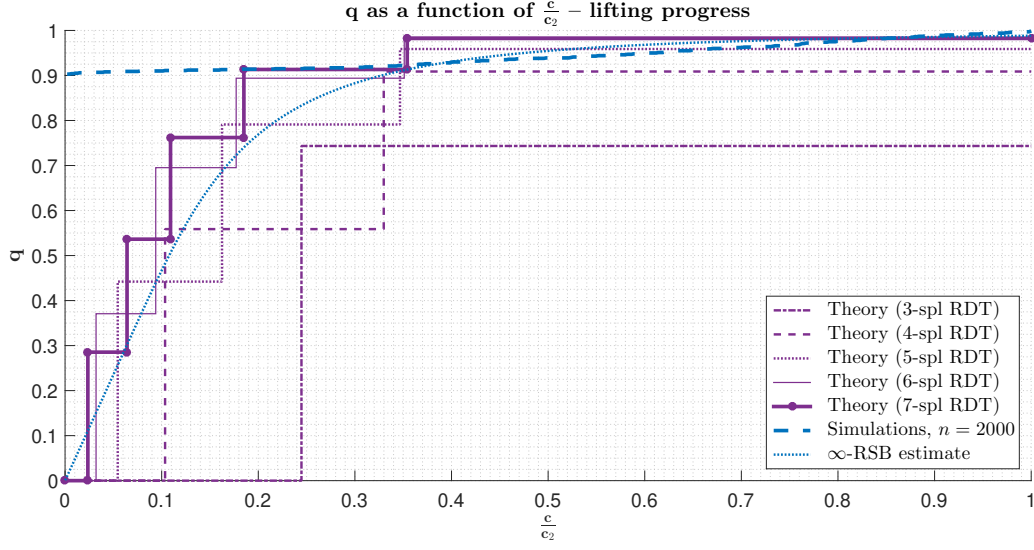


Figure 10: q overlap; SK model

- [67] M. Stojnic. A framework for performance characterization of *LASSO* algorithms. available online at <http://arxiv.org/abs/1303.7291>.
- [68] M. Stojnic. Various thresholds for ℓ_1 -optimization in compressed sensing. available online at <http://arxiv.org/abs/0907.3666>.
- [69] M. Stojnic. Recovery thresholds for ℓ_1 optimization in binary compressed sensing. *ISIT, IEEE International Symposium on Information Theory*, pages 1593 – 1597, 13-18 June 2010. Austin, TX.
- [70] M. Stojnic. Bounding ground state energy of Hopfield models. 2013. available online at <http://arxiv.org/abs/1306.3764>.
- [71] M. Stojnic. Lifting/lowering Hopfield models ground state energies. 2013. available online at <http://arxiv.org/abs/1306.3975>.
- [72] M. Stojnic. Controlled loosening-up (CLuP) – achieving *exact* MIMO ML in polynomial time. 2019. available online at <http://arxiv.org/abs/1909.01175>.
- [73] M. Stojnic. Sparse linear regression – CLuP achieves the ideal *exact* ml. 2020. available online at <http://arxiv.org/abs/2011.11550>.
- [74] M. Stojnic. Bilinearly indexed random processes – *stationarization* of fully lifted interpolation. 2023. available online at <http://arxiv.org/abs/2311.18097>.
- [75] M. Stojnic. Binary perceptrons capacity via fully lifted random duality theory. 2023. available online at <http://arxiv.org/abs/2312.00073>.
- [76] M. Stojnic. Fl rdt based ultimate lowering of the negative spherical perceptron capacity. 2023. available online at <http://arxiv.org/abs/2312.16531>.
- [77] M. Stojnic. Fully lifted interpolating comparisons of bilinearly indexed random processes. 2023. available online at <http://arxiv.org/abs/2311.18092>.
- [78] M. Stojnic. Fully lifted random duality theory. 2023. available online at <http://arxiv.org/abs/2312.00070>.
- [79] M. Stojnic. *Lifted* rdt based capacity analysis of the 1-hidden layer treelike *sign* perceptrons neural networks. 2023. available online at <http://arxiv.org/abs/2312.08257>.

- [80] M. Stojnic. Studying Hopfield models via fully lifted random duality theory. 2023. available online at <http://arxiv.org/abs/2312.00071>.
- [81] M. Stojnic. Capacity of the Hebbian-Hopfield network associative memory. 2024. available online at <http://arxiv.org/abs/2403.01907>.
- [82] M. Stojnic. A CLuP algorithm to practically achieve ~ 0.76 SK-model ground state free energy. 2025. available online at <http://arxiv.org/abs/2507.09247>.
- [83] M. Stojnic. Rare dense solutions clusters in asymmetric binary perceptrons – local entropy via fully lifted RDT. 2025. available online at <http://arxiv.org/abs/2506.19276>.
- [84] E Subag. The complexity of spherical p-spin models - A second moment approach. *Ann. Probab.*, 45:3385 – 3450, 2017.
- [85] E Subag. The geometry of the gibbs measure of pure spherical spin glasses. *Inventiones Mathematicae*, 210:135 – 209, 2017.
- [86] E Subag. Following the ground states of full-rsb spherical spin glasses. *Comm. Pure Appl. Math.*, 74:1021–1044, 2021.
- [87] E Subag. Free energy landscapes in spherical spin glasses. *Duke Math. J.*, 173:1291 – 1357, 2024.
- [88] M. Talagrand. Rigorous results for the Hopfield models with many patterns. *Prob. Theor. Rel. Fields*, 110:109–176, 1998.
- [89] M. Talagrand. The Parisi formula. *Annals of mathematics*, 163(2):221–263, 2006.
- [90] M. Talagrand. *Mean field models and spin glasse: Volume II*. A series of modern surveys in mathematics 55, Springer-Verlag, Berlin Heidelberg, 2011.
- [91] M. Talagrand. *Mean field models and spin glasses: Volume I*. A series of modern surveys in mathematics 54, Springer-Verlag, Berlin Heidelberg, 2011.
- [92] J. Y. Zhao. The Hopfield model with superlinearly many patterns. 2011. available online at <http://arxiv.org/abs/1108.4771>.